Cell Reports

Article

Active APPL1 sequestration by *Plasmodium* favors liver-stage development

Graphical abstract

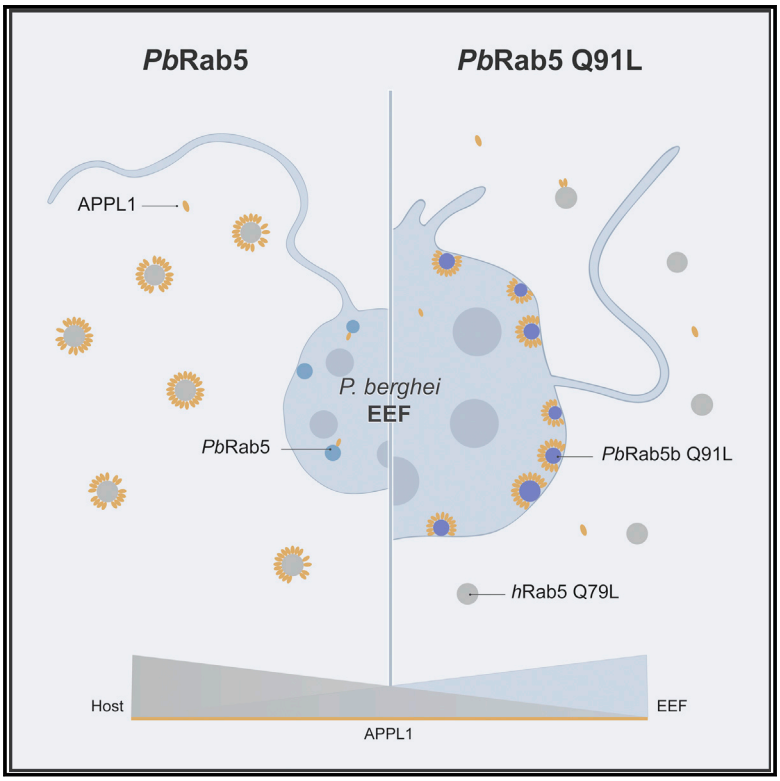

Authors

Aparajita Lahree,
Sara de Jesus Santos Baptista,
Sofia Marques, ..., Marino Zerial,
Varadharajan Sundaramurthy,
Maria M. Mota

Correspondence

mmota@medicina.ulisboa.pt

In brief

Lahree et al. demonstrate that *P. berghei* captures a host endosomal protein (APPL1) at the parasitophorous vacuole membrane (PVM) during liver-stage development, via an atypical parasite Rab-GTPase. Upon retention of APPL1 on host endosomes, parasite size is reduced, which can be rescued by re-enabling APPL1 enrichment on the parasite.

Highlights

- *P. berghei* exoerythrocytic forms (EEF) accumulate host APPL1 at the PVM
- *P. berghei* Rab5b interacts with APPL1 independent of other parasite proteins
- APPL1 retention on host endosomes correlates with reduction in parasite size

Lahree et al., 2022, Cell Reports *39*, 110886
May 31, 2022
https://doi.org/10.1016/j.celrep.2022.110886

CellPress

Cell Reports

CellPress
OPEN ACCESS

Article

Active APPL1 sequestration by *Plasmodium* favors liver-stage development

Aparajita Lahree,[1,2] Sara de Jesus Santos Baptista,[1] Sofia Marques,[1] Veronika Perschin,[3] Vanessa Zuzarte-Luís,[1] Manisha Goel,[4] Hadi Hasan Choudhary,[5] Satish Mishra,[5] Christian Stigloher,[3] Marino Zerial,[6] Varadharajan Sundaramurthy,[4] and Maria M. Mota[1,7,*]

[1]Instituto de Medicina Molecular- João Lobo Antunes (iMM-JLA), Faculdade de Medicina, Universidade de Lisboa, Av. Prof. Egas Moniz, 1649-028 Lisboa, Portugal

[2]Departamento de Bioengenharia, Instituto Superior Técnico, Av. Rovisco Pais 1, 1049-001 Lisboa, Portugal

[3]Imaging Core Facility, Biocenter, University of Würzburg, 97074 Würzburg, Germany

[4]National Centre for Biological Sciences, Tata Institute of Fundamental Research (NCBS), Bellary Road, Bangalore 560065, Karnataka, India

[5]CSIR-Central Drug Research Institute Sector 10, Jankipuram Extension, Sitapur Road, Lucknow 226031, Uttar Pradesh, India

[6]Max Planck Institute of Molecular Cell Biology and Genetics (MPI-CBG), Pfotenhauerstraße 108, 01307 Dresden, Germany

[7]Lead contact

*Correspondence: mmota@medicina.ulisboa.pt

https://doi.org/10.1016/j.celrep.2022.110886

SUMMARY

Intracellular pathogens manipulate host cells to survive and thrive. Cellular sensing and signaling pathways are among the key host machineries deregulated to favor infection. In this study, we show that liver-stage *Plasmodium* parasites compete with the host to sequester a host endosomal-adaptor protein (APPL1) known to regulate signaling in response to endocytosis. The enrichment of APPL1 at the parasitophorous vacuole membrane (PVM) involves an atypical *Plasmodium* Rab5 isoform (Rab5b). Depletion of host APPL1 alters neither the infection nor parasite development; however, upon overexpression of a GTPase-deficient host Rab5 mutant (*h*Rab5_Q79L), the parasites are smaller and their PVM is stripped of APPL1. Infection with the GTPase-deficient *Plasmodium berghei* Rab5b mutant (*Pb*Rab5b_Q91L) in this case rescues the PVM APPL1 signal and parasite size. In summary, we observe a robust correlation between the level of APPL1 retention at the PVM and parasite size during exoerythrocytic development.

INTRODUCTION

The malarial parasite *Plasmodium* undergoes obligatory intrahepatic development in mammals prior to initiating the erythrocytic infection cycle. Productive hepatocyte invasion is accompanied by the formation of a parasitophorous vacuole (PV) enclosing the parasite. The PV membrane (PVM) is critical for development of *Plasmodium* exoerythrocytic forms (EEFs), as it facilitates engagement with host organelles and proteins for tapping nutrients, blocking components of host selective autophagy (LC3, p62, NDP52, NBR1, Optineurin, and Rab7), and regulating the traffic of materials in and out of the parasite (Bano et al., 2007; Deschermeier et al., 2012; Itoe et al., 2014; Lopes da Silva et al., 2012; Meireles et al., 2017; Posfai et al., 2018; Real et al., 2018; Sá E Cunha et al., 2017; Thieleke-Matos et al., 2016). Infected hepatocytes present with an overall signaling deregulation, such as the upregulation of pro-survival factors (c-Met/HGF), downregulation of pro-apoptotic factors (p53, TNF-α, cytochrome *c*), suppression of metabolic regulators such as 5′- AMP activated protein kinase (AMPK), and desynchronization in Akt-mammalian target of rapamycin (mTOR) signaling (Glennon et al., 2019; Kaushansky et al., 2013; Leirião et al., 2005; Ruivo et al., 2016; Sand et al., 2005).

The hepatocyte's metabolic landscape is regulated by the endocytic network, through sorting of biomolecules for vectorial traffic and for cargo sensing and signaling (Schulze et al., 2019; Wang and Boyer, 2004; Zeigerer et al., 2015). Endosomal regulation of signal sensing and transduction is mediated through scaffold proteins (Murphy et al., 2009; Villaseñor et al., 2016), such as the regulation of Akt activity and substrate specificity by adaptor protein containing pleckstrin-homology (PH) domain (APPL1), phosphotyrosine-binding (PTB) domain, and leucine zipper motif 1 recruitment on a sub-population of early endosomes (EE), among others (Bohdanowicz et al., 2011; Goto-Silva et al., 2019; Kalaidzidis et al., 2015; Schenck et al., 2008). Akin to several intracellular pathogens, *Plasmodium* EEFs manipulate host endosomes to favor infection (Brumell and Scidmore, 2007; Romano et al., 2017). Host canonical autophagy pathway supports liver-stage infection, and late endosomes (LEs) act as sources of cholesterol for *Plasmodium* EEFs (Labaied et al., 2011; Lopes da Silva et al., 2012; Petersen et al., 2017). However, little is known about the role of other host endosomal components in remodeling of the infected cell.

Extending from previous reports about altered host signaling during *Plasmodium* exoerythrocytic infection (Glennon et al., 2019; Kaushansky et al., 2013; Ruivo et al., 2016), we sought

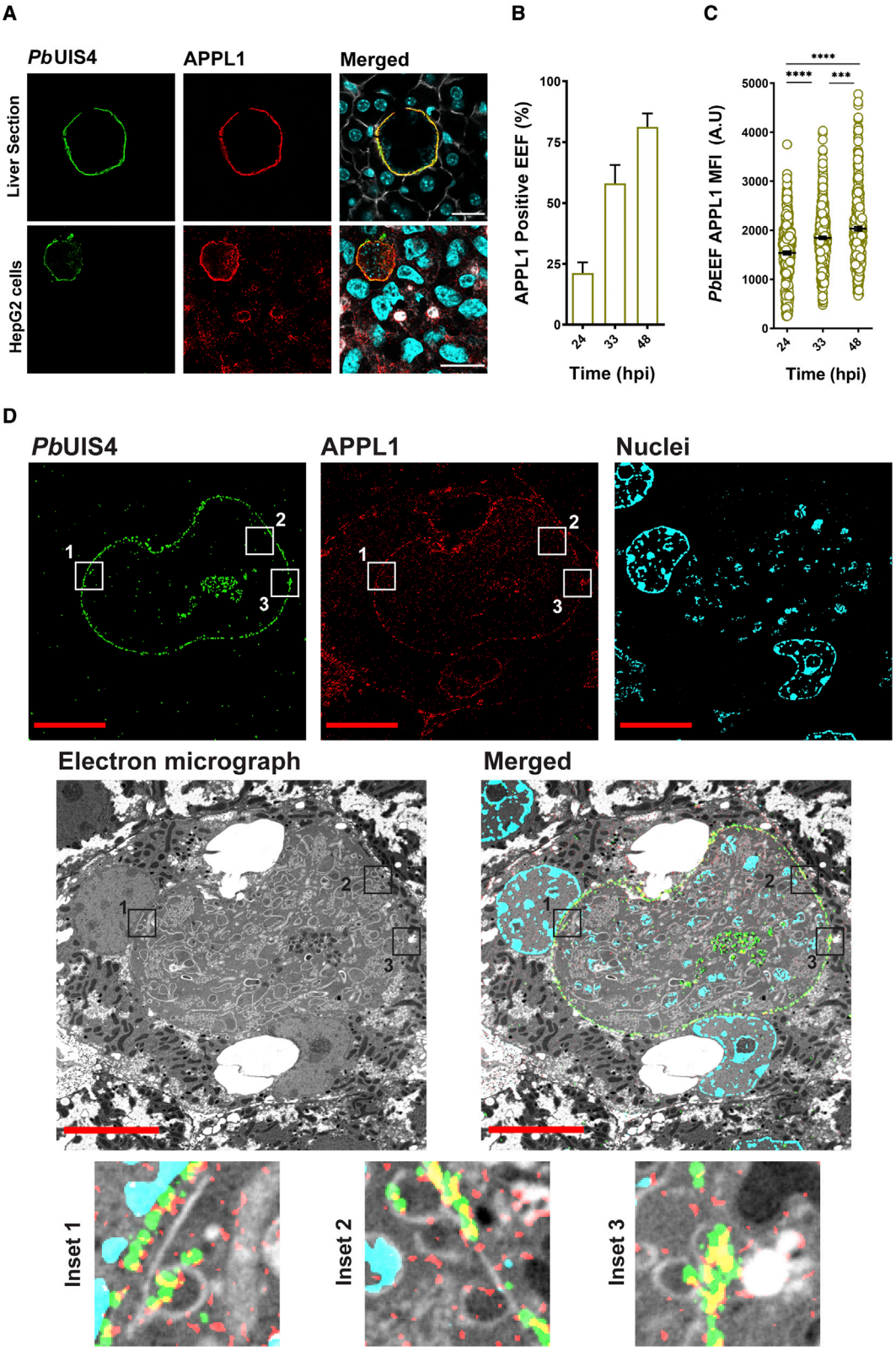

(legend on next page)

to explore whether *Plasmodium* manipulates scaffold proteins associated with host endosomes to facilitate the deregulation of host signaling pathways. In this study, we show the capture and sequestration of a host EE signaling scaffold, APPL1, at the PVM of *Plasmodium berghei* throughout exoerythrocytic development. APPL proteins contain a Bin/amphiphysin/RVS (BAR) domain, a PH domain, a PTB domain, and a leucine zipper motif 1. Recruitment of APPL to EE membrane occurs via interaction with Rab5 (GTP-bound state) (Miaczynska et al., 2004), whereupon APPL1 can interact with endocytosed receptors (Mao et al., 2006; Ryu et al., 2014) and subsequently recruit effectors to transduce molecular signals (Bohdanowicz et al., 2011; Zhou et al., 2009). The signaling proteins regulated by APPL1 include Akt, AMPK, and LKB1 (Bohdanowicz et al., 2011; Schenck et al., 2008; Zhou et al., 2009). APPL1 can also translocate to the nucleus upon interaction with Rab5, to regulate transcription (Banach-Orlowska et al., 2009; Rashid et al., 2009).

We observe that APPL1 deposition at the *P. berghei* PVM occurs independently of host Rab5 but depends on a parasite Rab5 isoform. Ectopic expression of a host Rab5 mutant (Q79L, lacking GTPase activity) results in the retention of APPL1 on host endosomes, leading to a stripping of its signal at the PVM together with a reduction in parasite size, both of which were rescued in parasites expressing the *Plasmodium* Rab5b Q91L isoform (also lacking its GTPase function). Overall, we identify an interaction between a host and a parasite protein from their vesicular trafficking pathway aimed at favoring infection.

RESULTS

APPL1 accumulates at the PVM throughout *P. berghei* liver-stage development

P. berghei (*Pb*GFP) EEF engage extensively with hepatocyte LE proteins, while host EE proteins have not been reported in the vicinity of EEFs (Lopes da Silva et al., 2012). We report a robust accumulation of the host EE adaptor APPL1 at the parasite periphery during exoerythrocytic development (Figure 1A). APPL1 appears enriched at the host-parasite interface both *in vivo* and *in vitro*, while lacking a signal of its classical recruiting component, host Rab5, there (Figure S1A, top panel). Furthermore, the frequency of APPL1-positive EEFs increased with parasite maturation (Figure 1B), as did the intensity of APPL1 around them, measured using the APPL1 fluorescence intensity signal at the EEF normalized to EEF area (mean fluorescence intensity [MFI]) (Figure 1C). An indirect validation of APPL1 signal around the parasite was obtained via detection of mRFP-tagged APPL1 around the EEF in transfected HepG2 cells 48 h post infection (hpi) (Figure S1B).

In vertebrates, APPL proteins exist in two isoforms, APPL1 and APPL2, which may form heterodimers (Miaczynska et al., 2004). While not functionally redundant, APPL1 and APPL2 share some similar roles (King et al., 2012; Tan et al., 2010). Hence, to discard a possible contribution of host APPL2 in Figure 1A, its localization was checked in *Pb*GFP-infected hepatocytes (Figure S1C). The absence of APPL2 signal around the EEF suggests that the enrichment was APPL1 specific. Notably, we detected the accumulation of APPL1 in another rodent malaria parasite, *Plasmodium yoelii*, albeit with visible signal in and around the EEF (Figure S1D).

To resolve the localization of APPL1 as either at the PVM or on docked APPL1-positive vesicles around the PVM, we employed correlative light and electron microscopy (CLEM) on *Pb*GFP-infected murine liver sections (48 hpi). APPL1 signal presented high proximity to the PVM-resident protein upregulated in sporozoites protein 4 (*Pb*UIS4) at the PVM (Figure 1D). To visualize whether this APPL1 population at the PVM was exposed to the host cytosol, partial permeabilization was performed in *P. berghei*-infected HepG2 cells (48 hpi). Incomplete saponin permeabilization of the parasite plasma membrane (PPM) corresponded to a loss in the cytosolic *Pb*HSP70 signal (Tsuji et al., 1994) and subsequently a decline in the PVM APPL1 signal relative to fully permeabilized EEFs (Figure S1E). Together, the CLEM analysis and partial permeabilization results confirmed that APPL1 is directly retained at the PVM and most of it is away from the host cytosol, respectively.

Parasite drives APPL1 deposition at the PVM independent of host endosomes

Despite the absence of a detectable host Rab5 signal at the PVM, we sought to understand whether it had an indirect role to activate and direct APPL1 to shuttle to the PVM. To that end, HepG2 cells were transiently transfected to express the human Rab5 (*h*Rab5) dominant-negative mutant S34N (Stenmark et al., 1994; Zhu et al., 2007) followed by infection with *Pb*GFP. No significant alteration in the APPL1 signal at the PVM (48 hpi) of EEFs could be observed in transfected cells relative to EEFs in untransfected cells (control) (Figures 2A and 2B).

Next, to address the role of the general host endosome traffic in APPL1 delivery at the PVM, a transient cytoskeletal destabilization was pharmacologically induced for disarraying host endosomes. Treatment with cytochalasin-D (Cyt-D, to destabilize the actin cytoskeleton) or nocodazole (NDZ, to depolymerize microtubules) led to the relocation of APPL1 to hepatocyte nucleus

Figure 1. Host EE protein APPL1 accumulates at the *P. berghei* PVM during exoerythrocytic development

*Pb*GFP-infected liver from C57BL6/J mice or cultured cells were immunostained for parasite PVM marker protein, *Pb*UIS4 (green), host APPL1 (red), actin (gray), and nuclei (cyan), at indicated time points in infection.

(A) Representative immunofluorescence (IF) micrograph indicating *Pb*UIS4 and APPL1 signals in infected murine liver cryosection (top) and human hepatoma cell line, HepG2 (bottom), at 48 hpi. Scale, 20 μm.

(B and C) Quantification of B APPL1-positive EEFs and C APPL1 signal (mean fluorescence intensity [MFI]) at the EEF at different time points in infection in HepG2 cells. Data represented as mean ± standard error of the mean (SEM).

(D) SIM and CLEM images of an infected hepatocyte (48 hpi) in a 100-nm liver section, immunostained for *Pb*UIS4, APPL1, and nuclei (cyan). Regions of interest are marked in boxes and zoomed as insets. Scale, 10 μm. (B and C) n = 370 (24 hpi), 512 (33 hpi), and 375 (48 hpi) EEFs counted in three independent experiments. ****$p < 0.0001$ and ***$p = 0.0002$ (unpaired t test with Welch correction). See also Figure S1.

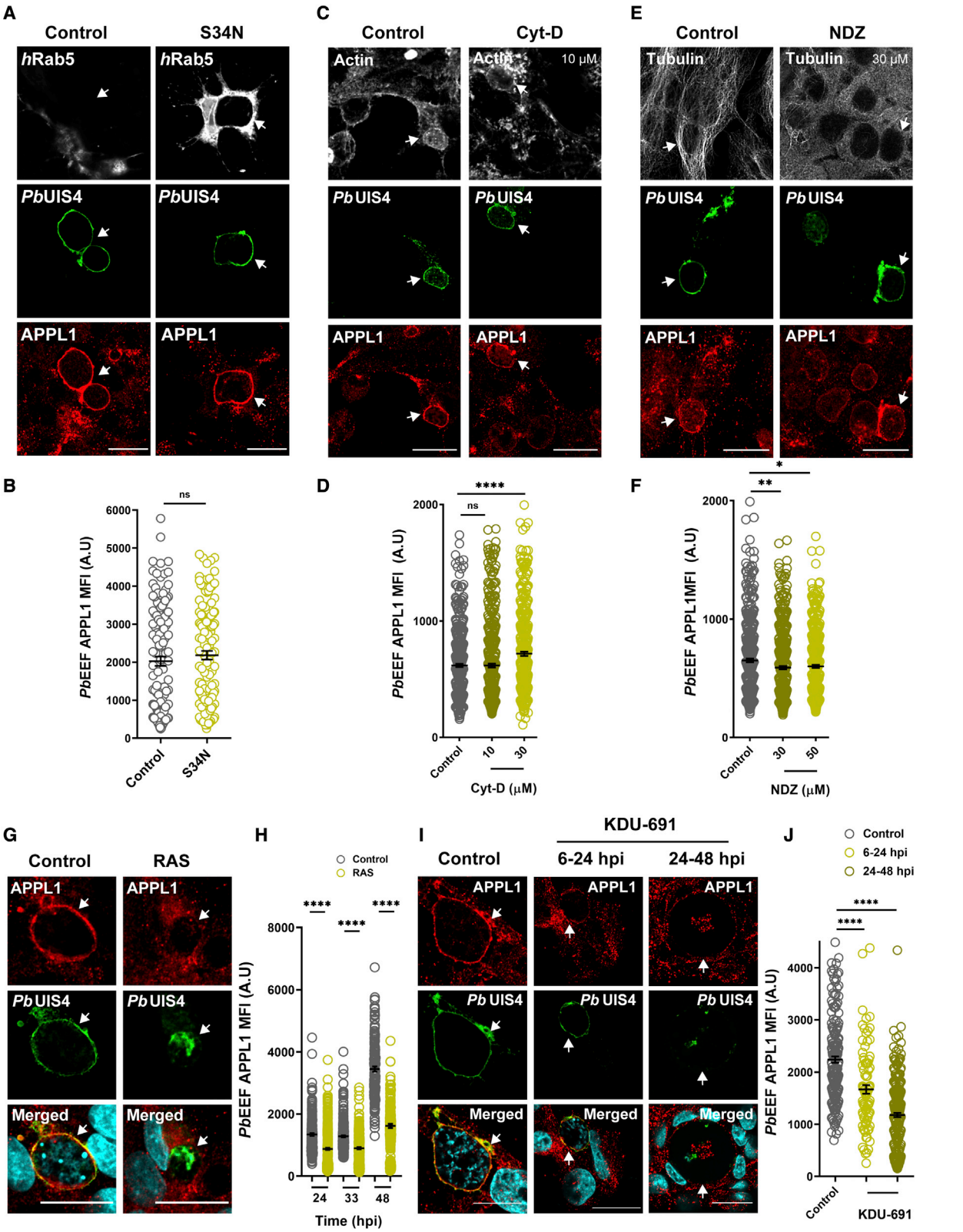

(legend on next page)

(Figure S1F), which has previously been reported in cells upon H_2O_2 exposure or epidermal growth factor (EGF) stimulation (Miaczynska et al., 2004). However, in Cyt-D-treated infected cells, the APPL1 signal at the PVM was similar to untreated control for 10 μM Cyt-D treatment and slightly higher upon 30 μM Cyt-D treatment, albeit not too drastic (Figures 2C and 2D). In the presence of NDZ, there was a slight but statistically significant reduction of the APPL1 signal at the PVM relative to untreated controls (Figures 2E and 2F). Collectively, these data suggested that the APPL1 localization to the PVM is not fully driven by host endosomal traffic to the PVM.

Having excluded *h*Rab5 and host endosomes as main contributors for APPL1 enrichment at the PVM, we hypothesized a direct parasite involvement in this process. We proceeded to investigate whether restricting parasite development would affect APPL1 accumulation at the PVM using γ-irradiated *Pb*GFP sporozoites (RASs) to infect HepG2 cells. RASs are invasion competent but incapable of intra-hepatic replication and maturation (Sigler et al., 1984) (Figure S1G). EEFs from RAS-infected cells exhibited a significant reduction in PVM APPL1 levels relative to control parasites (Figures 2G and 2H), indicating that APPL1 sequestration required a replication and translation competent EEF.

The dynamic replenishment of PVM-resident proteins from the parasite cytosol entails a successful *Plasmodium* hepatic development, as observed by Torin2-mediated blockade in PVM protein delivery (Hanson et al., 2013), albeit without a mechanism. *Plasmodium falciparum* PI4K (PFE0485w) was recently identified as a target of a Torin 2 derivative in blood stages (Krishnan et al., 2020), leading us to test whether the parasite-specific PI4K inhibitor KDU-691 (McNamara et al., 2013) would block PVM protein delivery and subsequently alter APPL1 signal there. KDU-691 phenocopied the interference of PVM protein traffic (Figure 2I) and was preferred over Torin2 to avoid possible inhibition of mTOR and related signaling in the host (Liu et al., 2012, 2013).

KDU-691 was used in two treatment regimes in infected cells to avoid complete EEF clearance and APPL1 signal was analyzed 48 hpi. KDU-691 was added either from 6 to 24 hpi (resulting in a smaller EEF area) or from 24 to 48 hpi (bloated EEFs with large area) (Figure S1H). KDU-691 treatment from 24 to 48 hpi displayed an evident reduction in APPL1 signal at the PVM (Figures 2I and 2J), whereas the 6–24 hpi-treated group demonstrated replenishment of *Pb*UIS4 at the PVM (Figure 2I) and a partial rescue of APPL1 there (Figures 2I and 2J). We hypothesize that a blockade of PVM proteins delivery with KDU-691 led to a progressive depletion of PVM proteins, therefore greatly reducing the EEF's ability to sequester APPL1. This could be partially reversed upon KDU-691 removal (6–24-hpi treatment regimen), enabling the gradual recovery of PVM proteins and the ability to sequester APPL1. This, we think, accounts for the intermediate level of APPL1 sequestration in the 6–24-hpi treatment group.

In conclusion, APPL1 enrichment at the PVM seems dependent on a parasite protein at the PVM and independent of host endosomes.

APPL1 at the PVM is in high proximity to a subpopulation of *P. berghei* Rab5b

Plasmodium spp. have neither a homolog of the vertebrate APPL1 protein nor any of its domains, but express a family of Rab-GTPases (Ward et al., 1997). *Plasmodium* Rab5 exists in three isoforms, with only the Rab5b isoform localizing to the PVM/PPM in addition to the parasite cytosol, during blood stages of infection (Ebine et al., 2016; Ezougou et al., 2014). Furthermore, Rab5b is refractory to deletion or functional replacement by the other Rab5 isoforms (Rab5a and Rab5c) in *P. falciparum* blood stages (Ebine et al., 2016; Ezougou et al., 2014; Quevillon et al., 2003), suggesting a distinct function from the other isoforms. The essentiality and localization of *Plasmodium* Rab5b encouraged exploration of the same in *P. berghei* liver stages as a putative candidate in capturing APPL1.

The cellular localization of *P. berghei* Rab5b (*Pb*Rab5b, PlasmoDB: PBANKA_1409100) during the liver stage was investigated using parasite lines expressing this protein with a C-terminal monomeric Azami-Green (*Pb*Rab5b_mAG) tag (Ebine et al., 2016) or 2× C-terminal hemagglutinin (HA)-tag (*Pb*Rab5b_HA, Figures S2A and S2B). The majority of the *Pb*Rab5b signal was

Figure 2. APPL1 enrichment at the PVM is driven by the parasite independently of the host machinery

HepG2 cells overexpressing the dominant-negative mutant of human Rab5 (*h*Rab5)-S34N were infected with *Pb*GFP parasites to quantify the APPL1 signal at the EEFs (arrow), 48 hpi in transfected and untransfected cells.

(A and B) (A) Representative IF micrograph indicating *h*Rab5 S34N (gray), APPL1 (red), and *Pb*UIS4 (green) in infected cells and (B) APPL1 signal (MFI) at the EEF in untransfected (control) or *h*Rab5 S34N-overexpressing cells. *Pb*GFP-infected HepG2 cells were transiently treated with cytoskeleton destabilization agents cytochalasin-D (Cyt-D) or nocodazole (NDZ), and at 33 hpi the APPL1 signal (red) around the EEF (arrow) was quantified.

(C and D) (C) Representative IF micrograph indicating actin (gray), *Pb*UIS4 (green), and APPL1 (red), and (D) APPL1 signal (MFI) at the EEF upon transient Cyt-D treatment in infected cells.

(E and F) (E) Representative IF micrograph indicating microtubules (tubulin, gray), *Pb*UIS4 (green), and APPL1 (red), and (F) APPL1 signal (MFI) at the EEF upon transient NDZ treatment of infected cells. Error bars represent ±SEM. To evaluate the role of parasite fitness in APPL1 enrichment, HepG2 cells were infected with either control or gamma-irradiated (RAS, 16 kRAD) *Pb*GFP sporozoites and immunolabeled for APPL1 (red) on the EEF (arrow) at indicated time points in infection.

(G and H) (G) Representative IF micrograph indicating APPL1 at the PVM (*Pb*UIS4, green) in infected cells, 48 hpi, and (H) APPL1 signal (MFI) at the EEF of control or RAS parasites throughout development. HepG2 cells infected with *Pb*GFP parasites were treated with either DMSO (control) or a *Plasmodium* PI-4-kinase inhibitor (KDU-691, 200 nM) either from 6 to 24 hpi or from 24 to 48 hpi to visualize the effect of PVM protein turnover on APPL1 (red) enrichment around the EEF (arrow), 48 hpi.

(I and J) (I) Representative IF micrograph showing APPL1 signal at the PVM (*Pb*UIS4, green), and (J) APPL1 signal quantification (MFI) at the EEF in KDU-691-treated infected cells. Data represented as mean ± SEM. Scale, 20 μm. (B) n = 133 (control) and 135 (S34N); (D) n = 462 (control), 477(10 μM Cyt-D) and 500 (30 μM Cyt-D); (F) n = 471 (control), 507 (30 μM NDZ) and 463 (50 μM NDZ); (H) n = 211 (control, 24 hpi), 340 (RAS, 24 hpi); 306 (control, 33 hpi), 259 (RAS, 33 hpi), 138 (control, 48 hpi), and 162 (RAS, 48 hpi); and (J) n = 210 (control), 88 (6–24 hpi), and 267 (24–48 hpi) EEFs counted in three independent experiments. ****$p < 0.0001$, **$p = 0.0029$, *$p = 0.0122$, and $^{n.s.}p = 0.3521$ (unpaired t test with Welch correction). See also Figure S1.

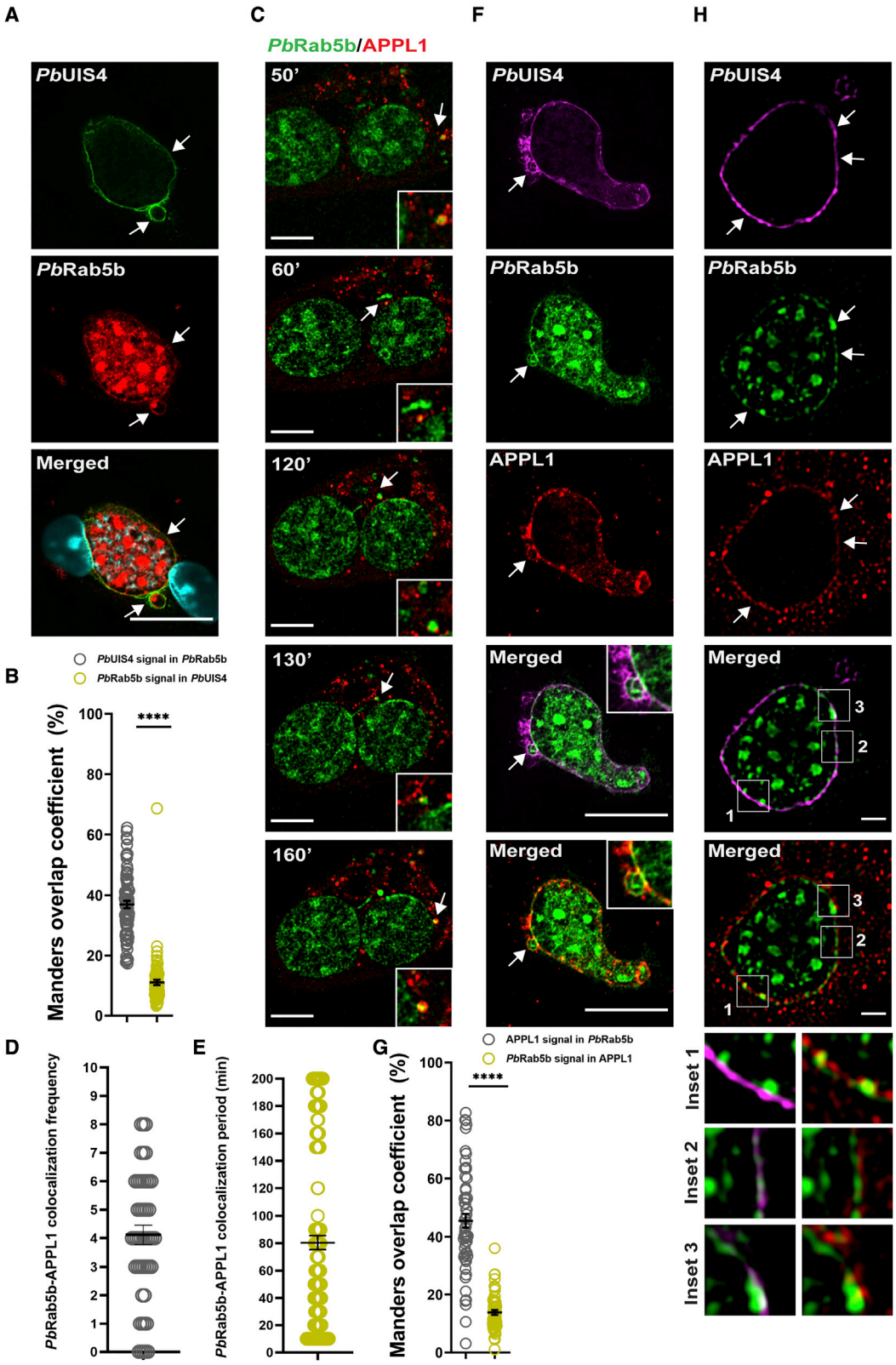

(legend on next page)

in the parasite cytosol with a small peripheral fraction detected in close proximity to the PVM and in the tubovesicular network (TVN) (Figures 3A and 3B). Mature EEFs presented a higher peripheral *Pb*Rab5b signal, and the overall signal also increased with EEF development (Figures S2C–S2E).

Live imaging of *Pb*Rab5b_mAG schizonts (45–48 hpi) in mRFP-APPL1-expressing HepG2 cells led to the identification of peripheral *Pb*Rab5b-positive structures engaging with APPL1-positive vesicles in the host cell (Figures 3C–3E and Videos S1 and S2). The same could be confirmed in *Pb*Rab5b_HA EEFs (48 hpi) via immunofluorescence (IF), where the peripheral *Pb*Rab5b signal was highly proximal to APPL1 signal along the PVM/TVN at that resolution (Figure 3F). Upon quantification, we observed that only a small fraction of *Pb*Rab5b colocalized with APPL1 at the parasite periphery in late schizonts (Mander's colocalization coefficient, Figure 3G). Again, mature schizonts had clearer peripheral *Pb*Rab5b-APPL1 signal proximity (Figures S2F–S2G). Through structured illumination microscopy (SIM), we could further visualize the discontinuous pattern of *Pb*Rab5b along the PVM (*Pb*UIS4 labeled), with some structures lying below *Pb*UIS4 and some in close proximity to or overlapping with the APPL1-positive structures in the vicinity (Figure 3H and insets).

While we could not conclude that *Pb*Rab5b always faces the host cytosol, a partial-permeabilization-based IF in HepG2 cells infected with *Pb*Rab5b_HA parasites was used to identify a PVM-proximal *Pb*Rab5b pool closely accessible from the host cytosol. Acetone-methanol-permeabilized (full permeabilization) EEFs displayed intracellular *Pb*Rab5b and cytosolic GFP staining, while 0.01% saponin (partial permeabilization)-treated EEFs lacked these cytosolic signals. However, in partially permeabilized cells, we noted a signal of *Pb*Rab5b around the PVM/TVN, which was discontinuous but present even in regions with low *Pb*UIS4 signal (Figure S2H).

Overall, there appeared to be a fraction of *Pb*Rab5b in close proximity to the PVM, providing for its peripheral pool between the PVM and PPM, which was close to the APPL1 signal there.

*Pb*Rab5b engages host APPL1 independently of other parasite components

The spatiotemporal proximity of APPL1 and *Pb*Rab5b signals at the PVM (Figures 1C and 3B) indicated a possibility of interaction. We explored this hypothesis through co-immunoprecipitation (coIP) studies in HepG2 cells infected with *Pb*Rab5b_HA parasites. APPL1 was immunoprecipitated from infected HepG2 cells and non-infected controls, followed by the probing of the IP fraction with anti-HA antibody. Given the scale of material used relative to the IF-based APPL1 and *Pb*Rab5b colocalization, unspecific signals were observed for both the non-infected (NI) and infected (INF) samples (Figure S4A, top blot). In the molecular weight range of *Pb*Rab5b (~24 kDa), however, a band in the INF lane just above the light-chain immunoglobulin (Ig) G band (running under 25-kDa mark) was detected, which was absent in the NI lane (Figures 4A and S3A, top blot). To validate this coIP *Pb*Rab5b signal in infected HepG2 cells and to exclude other parasite components as putative mediators, a transfection system was employed. HEK-293T cells were transfected with four different constructs: (1) a construct expressing HA only, (2) expressing the cytosolic domain of *Pb*UIS4_HA (~14 kDa, monomeric but runs around 27 kDa on PAGE) (M'Bana et al., 2021), (3) expressing *Pb*Rab5b_HA (~24 kDa), or (4) expressing the GTPase-deficient mutant-*Pb*Rab5b_Q91L_HA. These differently transfected cells were then subjected to APPL1 immunoprecipitation. Probing the IP fraction revealed a coIP of *Pb*Rab5b_HA and *Pb*Rba5b_Q91L_HA, but not of the cytosolic domain of *Pb*UIS4_HA (Figures 4B and S3B, top blot). This outlined that *Pb*Rab5b indeed engaged with APPL1, and independently of other parasite proteins, albeit with possible indirect interaction via other host components.

Given that *Pb*Rab5b gene deletion is lethal in *Plasmodium* blood stages, further exploration of its role in APPL1 recruitment during EEF development was performed using orthologous expression models. First, we visualized the localization of HA-tagged *Pb*Rab5b variants (wild type [WT] and Q91L mutant) upon exogenous expression in HepG2 cells. The Q91L mutation in *Pb*Rab5b is similar to the Q79L mutation in the human Rab5 (*h*Rab5), which renders it GTPase deficient, leading to a prolonged GTP-bound state (Ebine et al., 2016; Stenmark et al., 1994; Taku et al., 2021). The *h*Rab5_Q79L mutant was shown to accumulate APPL1 upon expression in cells (Kalaidzidis et al., 2015; Miaczynska et al., 2004; Zhu et al., 2007).

*Pb*Rab5b_HA and *Pb*Rab5b_Q91L_HA could be detected throughout the cell with a sub-population appearing punctuate

Figure 3. A sub-population of *P. berghei* Rab5b is detected at the PVM and co-localizes with APPL1 in some regions

Rab5b localization in *P. berghei* EEFs was assessed using a parasite line expressing *Pb*Rab5b fused to 2x-HA-tag at the C terminus (*Pb*Rba5b_HA). HepG2 cells infected with *Pb*Rba5b_HA parasites were immunostained at indicated time points in infection to visualize *Pb*Rab5b_HA, *Pb*UIS4, and nuclei (cyan).

(A) Representative IF micrograph showing *Pb*Rab5b (red) and *Pb*UIS4 (green) localization at 48 hpi. Arrows indicate PVM regions positive for *Pb*Rab5b. Scale, 20 μm.

(B) Manders colocalization coefficient of overlap between *Pb*UIS4 and *Pb*Rab5b signals in *Pb*Rab5b_HA parasites, 48hpi. To observe spatial colocalization of *Pb*Rab5b with APPL1, either live imaging or IF was used to visualize APPL1 and *Pb*Rab5b. HepG2 cells expressing mRFP-APPL1 were infected with parasites expressing monomeric Azami-Green-tagged *Pb*Rab5b (*Pb*Rab5b_mAG) to visualize protein dynamics in live confocal acquisition from 45 to 48 hpi.

(C–E) (C) Representative frames at indicated time points showing live mRFP-APPL1 (red) and *Pb*Rab5b_mAG (green) signals, (D) frequency of APPL1-*Pb*Rab5b double-positive events, and (E) the lifetime (period) of APPL1-*Pb*Rab5b double-positive events in transfected-infected cells over acquisition period. Arrows indicate insets. Scale, 10 μm.

(F and G) (F) Representative IF micrographs indicating *Pb*UIS4 (magenta), *Pb*Rab5b (green), APPL1 (red), and (G) Manders colocalization coefficient of overlap between APPL1 and *Pb*Rab5b signals at *Pb*Rab5b_HA EEFs in HepG2 cells, 48 hpi. Arrow indicates insets. Scale, 20 μm.

(H) SIM image identifying domain like distribution of APPL1 (red) and *Pb*Rab5b (green) around the PVM (*Pb*UIS4, magenta). Arrows indicate insets. Scale, 2 μm.

Data represented as mean ± SEM. (B) n = 78, (D) n = 51, (E) n = 189 events, and (G) n = 56, EEFs counted in three independent experiments. ****$p < 0.0001$ (unpaired t test with Welch correction). See also Figure S2.

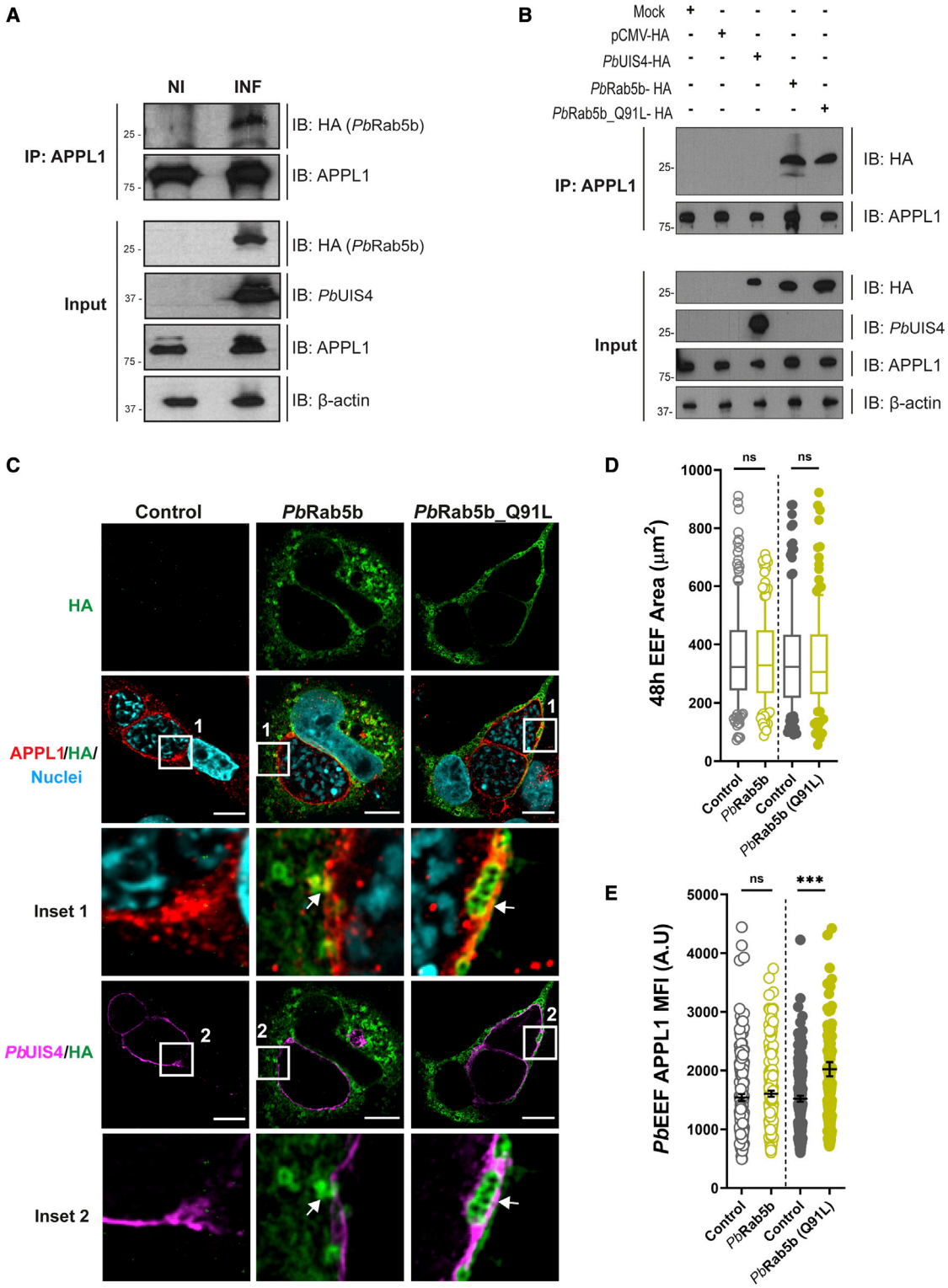

Figure 4. *Pb*Rab5b engages host APPL1 independently of other parasite factors

Protein-protein interaction between APPL1 and *Pb*Rab5b was indirectly observed via co-immunoprecipitation in HepG2 cells infected with *Pb*Rab5b-HA parasites, or in HEK-293T cells overexpressing codon optimized *Pb*Rab5b variants (WT and Q91L).

(legend continued on next page)

or slightly tubular, without any drastic alterations in the overall APPL1 distribution in the cell (Figure S4A).

Next, we assessed if exogenous *Pb*Rab5b variants would affect the PVM APPL1 enrichment in transfected and infected HepG2 cells. The EEFs in transfected cells presented with some *Pb*Rab5b_Q91L_HA-positive structures at the PVM surrounded by APPL1 (Figure 4C, column 3, insets 1 and 2), while *Pb*Rab5b_HA could be found in vesicular structures in the host cytosol and, at times, in proximity to APPL1 at the TVN (Figure 4C, column 2, insets 1 and 2). There was no alteration in parasite size (48 hpi) (Figure 4D); however, there was an increase in the APPL1 signal at the PVM of parasites in cells expressing *Pb*Rab5b_Q91L_HA, relative to parasites in untransfected cells, or in those expressing *Pb*Rab5b_HA (Figure 4E). As the Q91L mutation leads to GTPase deficiency in *Pb*Rab5b, the increase in APPL1 at the PVM of parasites in cells exogenously expressing *Pb*Rab5b_Q91L led us to hypothesize that the Q91L mutant could also retain APPL1 on membrane longer than WT *Pb*Rab5b. Overall, *Pb*Rab5b variants could be detected on host membranous structures upon expression in host cells, while, in the case of the mutant, we could also observe homing of vesicles positive for *Pb*Rab5b_Q91L to the PVM, and an elevation in the APPL1 signal there in the presence of the parasite. Whether parasites expressing *Pb*Rab5b_Q91L present with elevated APPL1 at the PVM relative to WT EEF is explored in later sections.

Altogether, *Pb*Rab5b interacts, directly or indirectly, with host APPL1 and seems to be the parasite protein responsible for APPL1 sequestration into the PVM.

APPL1 deficiency does not affect liver-stage *Plasmodium* infection

A key conundrum so far was the biological purpose of APPL1 sequestration by the EEF. To evaluate the role of host APPL1 on *P. berghei* liver-stage infection *in vitro*, small hairpin RNA (shRNA)-mediated knockdown (KD) of APPL1 was induced in HepG2 cells (Figure S3B) followed by infection with *Pb*GFP sporozoites. We observed comparable parasite sizes at 48 hpi between the different shRNA-expressing cells relative to non-target control (NT, Figure S3C), while the parasite load at 48 hpi displayed a different trend. Two of the three shRNA-expressing HepG2 cells presented with higher parasite load relative to NT cells (Figure S3D). Since the efficiency of APPL1 KD in shRNA #55 was comparable with that in shRNA# 53-expressing cells, and better than what was observed for shRNA #54, a difference in the parasite load pattern was suspected for off-target effects in this system. Hence, we replicated the *Pb*GFP infection experiments in C57BL6/J mice models either WT (APPL1$^{+/+}$) or APPL1 knockout (APPL1$^{-/-}$) (Figure S3E). We did not observe significant differences between the two groups of animals regarding parasite liver load (Figure 5A), although a mild increase in parasite size (Figure 5B) was observed in APPL1$^{-/-}$ animals relative to APPL1$^{+/+}$. Altered EEF size was not biologically relevant given the lack of difference in survival profiles (Figure 5C) and blood parasitemia levels (Figure S3F) during the ensuing blood-stage infection between the two groups of infected mice.

APPL1 retention on host EE robustly correlates with reduction in EEF size

The depletion of host APPL1 did not yield clear effects on *P. berghei* intra-hepatic infection, leading to an alternative hypothesis that removal of APPL1 by the parasite is aimed at depleting a host signaling adaptor, possibly to compromise defenses against the pathogen.

To test this hypothesis, we promoted the preferential retention APPL1 on host EE and observed its effects on parasite development. HepG2 cells expressing the GTPase-deficient *h*Rab5 mutant (*h*Rab5_Q79L, GTP-bound state) were infected with *Pb*GFP sporozoites followed by measuring the PVM APPL1 signal and EEF area in untransfected and transfected cells (Figure 5D). *h*Rab5_Q79L-expressing cells presented with enlarged endosomes (Miaczynska et al., 2004) enriched for APPL1 (Figures 5D and 5G, yellow arrows). The PVM APPL1 signal and the size of EEFs in these cells were reduced relative to parasites in untransfected cells (Figures 5E and 5F). The retention of APPL1 on host endosomes and not the PVM therefore correlated with a reduction in parasite size, indicating a possibility that APPL1 removal from the host may favor parasite development.

To validate whether the loss of PVM APPL1 is what leads to a reduction in EEF size, HepG2 cells were infected with *P. berghei* parasites, expressing either the WT or the GTPase-deficient mutant (Q91L) of *Pb*Rab5b. In WT HepG2 cells, *Pb*Rab5b_Q91L parasites have lower overall *Pb*Rab5b signal relative to WT EEFs (Figures S5A and S5B) but maintain relatively similar EEF sizes over development (Figure S5C). There was also no difference in the parasite load at 48 hpi between the two parasite lines in HepG2 cells (Figure S5D). However, there were differential APPL1 enrichment dynamics at the PVM between these two parasite lines over development. While the *Pb*Rab5b_Q91L mutant had higher APPL1 signal in early schizonts (24 hpi)

(A) APPL1 was immunoprecipitated in *Pb*Rab5b_HA infected cells (INF) and non-infected controls (NI) at 48 hpi. Proteins from the IP fractions were immunoblotted against the HA-tag (*Pb*Rab5b_HA, 24 kDa) and APPL1 (80 kDa). The pre-IP (input) fraction was probed for the HA-tag, *Pb*UIS4 (25 kDa), APPL1, and β-actin (42 kDa) respectively.

(B) HEK-293T cells either untransfected (lane 1) or transfected with pCMV-HA (lane 2) or *Pb*UIS4 (cytosolic domain)-HA (lane 3) or *Pb*Rab5b_HA (lane 4) or *Pb*Rab5b_Q91L_HA (lane 5) expressing constructs were prepared for immunoprecipitation of APPL1 48 h post transfection. Proteins from the IP fractions were probed for the HA-tag and APPL1. The pre-IP (input) fraction was probed for the HA-tag, *Pb*UIS4 (cytosolic domain, ~14 kDa monomeric), APPL1, and β-actin respectively. HepG2 cells were transfected with codon optimized variants of HA-tagged *Pb*Rab5b (WT or Q91L GTPase-deficient mutant), followed by infection with *P. berghei* parasites to observe the contribution of exogenous *Pb*Rab5b (*Pb*Rab5b_HA) on the APPL1 enrichment at the EEF.

(C–E) (C) Representative IF micrograph indicating exogenous *Pb*Rab5b_HA (WT or Q91L, green), APPL1 (red), and *Pb*UIS4 (magenta); (D) EEF area; and (E) APPL1 signal quantification (MFI) at the EEF in transfected and untransfected cells. Boxed regions are zoomed insets and arrows indicate regions of close proximity between respective signals in the frame. Scale, 20 μm. (D and E) n = 161 (control_*Pb*Rab5b), 161 (*Pb*Rab5b), and 145 (control_*Pb*Rab5b_Q91L), 135 (*Pb*Rab5b_Q91L); boxplot borders indicate the 10th and 90th percentiles. Data represented as mean ± SEM. $^{n.s.}$p = 0.5480 (*Pb*Rab5b, D) and $^{n.s.}$p = 0.7696 (*Pb*Rab5b_Q91L, D); $^{n.s.}$p = 0.7639 (*Pb*Rab5b, E); **p = 0.0073 (unpaired t test with Welch correction. See also Figure S3.

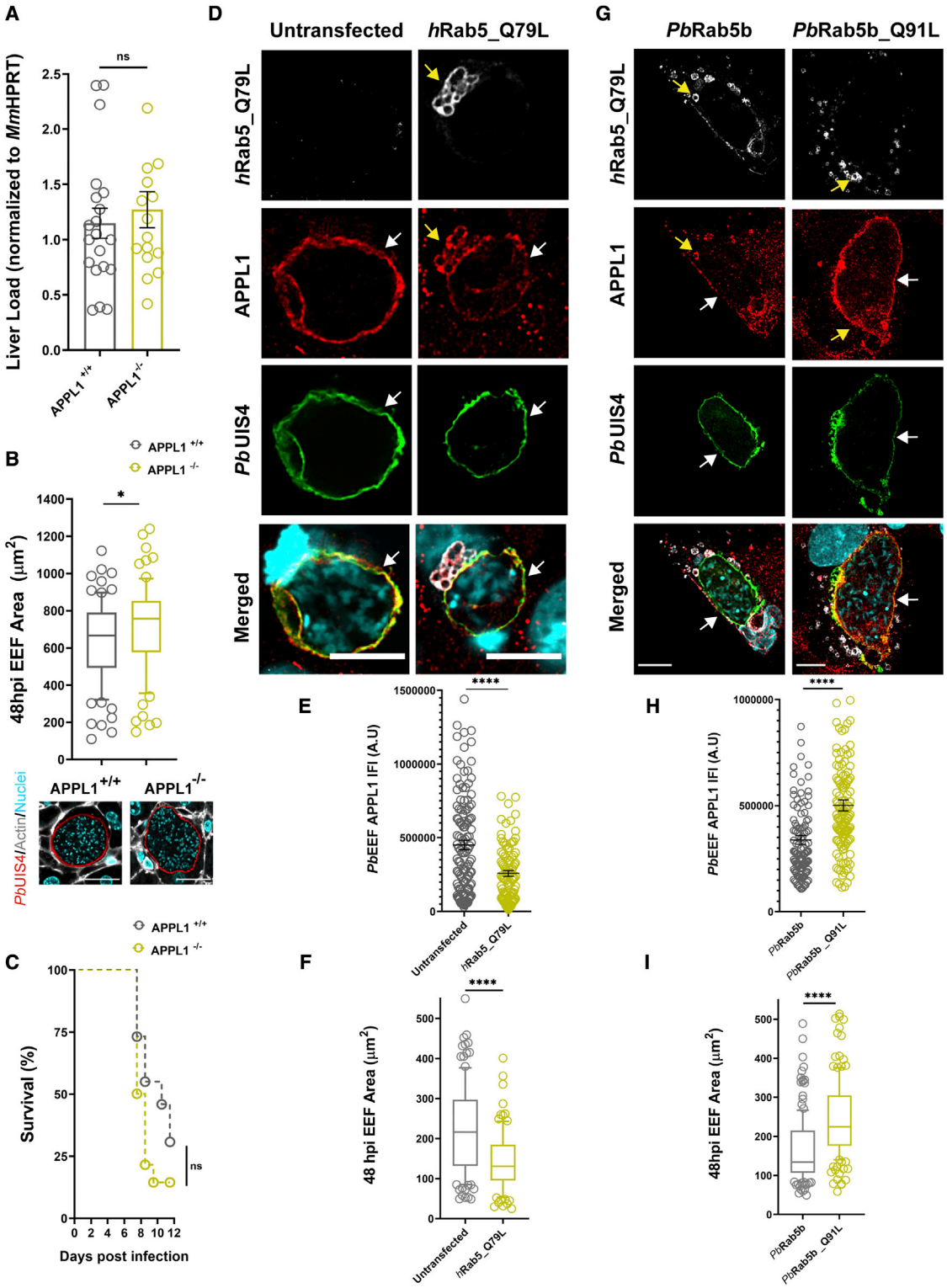

Figure 5. APPL1 sequestration on host endosomes but not its deficiency negatively affects EEF development

Effect of host APPL1 depletion on *Pb*GFP infection was tested in C57BL6/J mice, either WT (APPL1$^{+/+}$) or knockout for APPL1 (APPL1$^{-/-}$). Intravenous injection of 50,000 *Pb*GFP sporozoites was followed by collection of infected murine livers at 48 hpi, and processing for real-time quantitative PCR (qRT-PCR) or IF staining. Survival of infected mice was assessed upon parasite egress from the liver to initiate blood-stage infection.

(A) Liver burden of infection (liver load, *Pb18s* rRNA) quantified through qRT-PCR (normalized to mouse *hprt-Mm*HPRT).

(legend continued on next page)

relative to the WT EEFs, the difference was reversed at 48 hpi (Figures S5E and S5F). Overall, *Pb*Rab5b WT EEFs demonstrated a sharper elevation in APPL1 enrichment at the PVM over development than *Pb*Rab5b_Q91L mutants, leading us to associate the GTP binding of *Pb*Rab5b as a factor affecting APPL1 capture and sequestration at the PVM.

Now, in the presence of *h*Rab5_Q79L in the host cell, *Pb*Rab5b _Q91L parasites demonstrated higher levels of PVM APPL1 signal compared with WT parasites, which expectedly exhibited reduced APPL1 signal (Figures 5G and 5H). Furthermore, *Pb*Rab5b _Q91L EEFs could also rescue the EEF size, while *Pb*Rab5b parasites were smaller in the presence of *h*Rab5_Q79L (Figure 5I). The rescue in EEF size also correlated with the rescue of the PVM APPL1 signal in *Pb*Rab5b_Q91L parasites, indicating some relationship between removal of APPL1 from the host cytosol and favorable parasite development, although the mechanism of the same and the contribution of other players remain to be explored.

APPL1 has been described as a signaling adaptor and its function to be dependent on its interaction with Rab5 (Miaczynska et al., 2004). We were hence keen to understand whether the retention of APPL1 on *h*Rab5_Q79L endosomes in transfected cells led to alterations in the activation/inactivation status of APPL1 downstream effectors and if any of these alterations may hint toward a possible explanation for the reduction in EEF size as noted in Figure 5F. The phosphorylation status of some APPL1 downstream effectors such as Akt, GSK-3β, and AMPK (Cheng et al., 2007; Schenck et al., 2008) was monitored in HEK-293T cells transfected with constructs expressing either mCherry tag only (mock) or mCherry_*h*Rab5_Q79L or *Pb*Rab5b or *Pb*Rab5b_Q91L (Figures S6G and S6H). We observed an elevation in the phosphorylation of host Akt (S473) in all groups expressing Rab5 variants relative to mock (Figures S6A–S6C), while no significant difference could be observed in the phosphorylation of GSK-3β (S9), which is downstream of Akt (Figures S6A, S6B, and S6D) (Grabinski and Kanaan, 2016). Curiously, an elevation in the phosphorylation of AMPK (T172) was observed solely for *h*Rab5_Q79L-expressing cells (Figures S6A, S6B, and S6E) relative to mock cells. The differential status of AMPK phosphorylation piqued our interest, given a previous report identifying host AMPK activation as detrimental to *Plasmodium* EEF development in hepatocytes (Ruivo et al., 2016). There is also growing evidence of the role of APPL1 in regulating AMPK activation (Dadson et al., 2014; Sayeed et al., 2018; Zhou et al., 2009). While *h*Rab5_Q79L overexpression may present with several alterations in the host, the activation of AMPK appeared intriguing considering the previously observed correlation between EEF size and APPL1 PVM localization, although more exploration would be required to definitively attribute APPL1 as the key player regulating parasite development in hepatocytes.

DISCUSSION

As an intracellular obligatory parasite, *Plasmodium* manipulates its host cell to facilitate infection. *Plasmodium* EEFs were shown to siphon host biomolecules while evading autophagic clearance through exclusion of host phagophore components (Agop-Nersesian et al., 2017; De Niz et al., 2020; Fougère et al., 2016; Itoe et al., 2014; Lopes da Silva et al., 2012; Meireles et al., 2017; Petersen et al., 2017; Posfai et al., 2018; Real et al., 2018; Thieleke-Matos et al., 2016; Vijayan et al., 2020). Likewise, a deregulation of host homeostatic pathways was described in *Plasmodium*-infected hepatocytes, which includes a desynchronization in host RPS6 phosphorylation upon insulin stimulation (Glennon et al., 2019; Kaushansky et al., 2013) and the suppression of AMPK activity despite nutrient loss in the host (Ruivo et al., 2016). Bearing in mind the endosomal regulation of the Akt-mTOR and the AMPK pathways (Sigismund et al., 2012; Villaseñor et al., 2016), we sought to explore whether *Plasmodium* EEFs manipulate hepatocyte adaptor proteins associated with endosomal signaling.

Intracellular pathogens often exploit adaptor proteins to hijack a host machinery to enable entry or establishment (Dokainish et al., 2007; Martinez-Quiles et al., 2014; Pielage et al., 2008; Yuan et al., 2005). The role of host signaling adaptors in infections with Apicomplexan parasites, however, remains obscure. The present study describes a *Plasmodium*-mediated capture and sequestration of a host EE adaptor protein-APPL1 at the PVM through an atypical parasite Rab5 isoform (Rab5b). Akin to observations in *P. falciparum* Rab5b (Ebine et al., 2016; Ezougou et al., 2014), a fraction of the *P. berghei* Rab5b

(B) Box and whisker plot indicating EEF area, estimated from liver sections immunostained for *Pb*UIS4 (red), actin (gray), and nuclei (cyan). Representative IF micrographs used for measurements are shown below the plot. Box borders represent the 10th and 90th percentiles; scale, 20 μm.

(C) Kaplan-Meier survival curves for infected APPL1$^{+/+}$ or APPL1$^{-/-}$ mice. Effect of the inability of the EEF to enrich APPL1 at the PVM on parasite development was assessed in *Pb*GFP-infected HepG2 cells overexpressing the human Rab5 GTPase-deficient mutant *h*Rab5_Q79L. Samples were immunolabeled for *h*Rab5_Q79L (mCherry tag, gray), APPL1 (red), and *Pb*UIS4 (green), 48 hpi. *h*Rab5_Q79L-positive endosomes retain APPL1 on enlarged endosomes (yellow arrow).

(D) Representative IF micrographs indicating APPL1 around the EEF (white arrow) in untransfected and transfected cells (labels on top of panels).

(E and F) (E) APPL1 signal quantification (integral fluorescence intensity [IFI]) at the EEF, and (F) EEF area in untransfected and transfected cells. *h*Rab5_Q79L-expressing cells were infected with parasites expressing either WT (*Pb*Rab5b, column 1 label) or the GTPase-deficient mutant of *P. berghei* Rab5b (*Pb*Rab5b_Q91L, column 2 label) to quantify APPL1 signal at their PVM (*Pb*UIS4, green).

(G–I) (G) Representative IF micrographs indicating APPL1 (red) around the EEF (*Pb*UIS4, green), (H) APPL1 signal (IFI) at the EEF, and (I) EEF area of *Pb*Rab5b and *Pb*Rab5b_Q91L parasites in *h*Rab5_Q79L-expressing host cells. White arrows indicate parasite location and yellow arrows highlight enlarged *h*Rab5_Q79L-positive endosomes. Scale, 10 μm. Data represented as mean ±SEM. (A) n = 20 (APPL1$^{+/+}$) and n = 16 (APPL1$^{-/-}$) mice, (B) n = 86 (APPL1$^{+/+}$) and n = 72 (APPL1$^{-/-}$) EEFs, and (C) n = 12 (APPL1$^{+/+}$) and n = 14 (APPL1$^{-/-}$) mice, examined in three independent experiments. (E and F) n = 124 (untransfected) and 94 (*h*Rab5_Q79L), (H and I) n = 117 (*Pb*Rab5b) and 127 (*Pb*Rab5b_Q91L) EEFs counted in three independent experiments. $^{n.s.}$p = 0.5550, unpaired t test with Welch correction (A), *p = 0.0286, Mann-Whitney U-test (B), and $^{n.s.}$p = 0.1404, Log rank (Mantel-Cox) test (C). ****p < 0.0001, unpaired t test with Welch correction (E, F, H, and I). See also Figure S3.

(PlasmoDB: PBANKA_1409100, *Pb*Rab5b) was found to localize at the EEF periphery, where *Pb*Rab5b was distributed in discontinuous domains on or under the PVM, in close proximity to APPL1-positive structures. *Pb*Rab5b co-immunoprecipitated with APPL1 from infected cells, as well as in cells transfected with constructs exogenously expressing *Pb*Rab5b variants (WT and Q91L), the latter model indicating the non-requirement of other parasite components in engaging APPL1. Infection of cells or mice deficient in APPL1 led to no major alterations in parasite growth or survival.

Unlike the mammalian Rab-GTPases, which possess a C-terminal prenylation motif, essential for membrane access (Wang and Casey, 2016), *Plasmodium* Rab5b instead contains an N-terminal myristoylation motif, necessary for membrane localization, reminiscent of the plant Rab5-like protein-Ara6 (Ezougou et al., 2014; Ueda et al., 2001). Thus, the localization of the exogenous *Pb*Rab5b variants to membranous structures in the host cells, and its interaction with APPL1, hinted toward a possible role of other host proteins in enabling the same.

Upon infecting host cells exogenously expressing *Pb*Rab5b variants, we observed an elevation in the APPL1 signal at the PVM of parasites in *Pb*Rab5b_Q91L-expressing HepG2 cells relative to EEFs in untransfected controls and cells expressing WT *Pb*Rab5b. Furthermore, structures positive for *Pb*Ra5b_Q91L could be detected at the PVM together with APPL1, and to some extent also for the exogenous WT *Pb*Rab5b. While only suggestive, there appeared to be a mechanism of homing of the *Pb*Rab5b structures to the PVM and a synergy toward APPL1 delivery there, which, together with the live imaging data of *Pb*Rab5b_mAG dynamics (Figure 3C), suggested that *Pb*Rab5b may be released in vesicles or through the PVM/TVN to the host cytosol and can return to the EEF. This may serve to capture APPL1 and deliver it at the PVM, conceivably together with other host proteins. The local lipid composition and lipid modifications on interacting proteins may also contribute to these events.

*Pb*Rab5b lacks the classical PEXEL or VTS motifs for parasite protein export to the PVM/host cytosol (Hiller et al., 2004; Marti et al., 2004). However, N-myristoylated parasite proteins lacking the PEXEL motif, such as *P. falciparum* adenylate kinase 2 (*Pf*AK2), were shown to traffic to the parasite periphery employing post-translational modification like myristoylation, palmitoylation, and a cluster of lysine residues (Ebine et al., 2016; Ezougou et al., 2014; Möskes et al., 2004; Ridzuan et al., 2012; Thavayogarajah et al., 2015). The *Leishmania* protein HASPB also shows a similar N-myristoylation/palmitoylation-dependent export (Denny et al., 2000).

The purpose of APPL1 removal from the host cytosol and its retention at the PVM remained indirect, as hosts deficient in APPL1 demonstrated no stark alteration in parasite development or infection, leading us to hypothesize that APPL1 removal was aimed at creating a deficiency of this adaptor in the host. If APPL1 took part in host responses against infection, it may be detrimental to EEF development. APPL1 retention on host EE upon *h*Rab5_Q79L expression in HepG2 cells (Miaczynska et al., 2004) led to stripping of the PVM APPL1 signal on EEFs in transfected cells, together with a reduction of parasite size. Principally, this may be a pleiotropic effect of *h*Rab5_Q79L overexpression in host cells independent of APPL1, and likely similar for different parasite lines. However, upon infecting *h*Rab5_Q79L-expressing cells with *P. berghei* parasites expressing the GTPase-deficient mutant of *Pb*Rab5b (*Pb*Rab5b_Q91L), the PVM APPL1 signal and the EEF size were rescued relative to WT parasites. First, this led us to infer that APPL1 retention on host EE was indeed detrimental to EEF growth, although we cannot fully exclude other effects of *h*Rab5_Q79L expression. Second, to indirectly explain the effect on parasite size upon APPL1 sequestration on *h*Rab5_Q79L-positive endosomes, we proceeded to visualize the activation/inactivation status of kinases downstream of APPL1. Irrespective of infection, cells expressing either *h*Rab5_Q79L or the *Pb*Rab5b variants demonstrated elevation in the phosphorylation of Akt but not of its downstream kinase- GSK-3β. The phosphorylation of another APPL1 effector kinase-AMPK was elevated only in *h*Rab5_Q79L-expressing cells and not the *Pb*Rab5b variants, which was particularly interesting given previous studies indicating the negative effect of AMPK activation on EEF size (Ruivo et al., 2016). A reduction in the activity of AMPK upon depletion of APPL1 was previously demonstrated (Zhou et al., 2009), while APPL1 has been associated with the negative regulation of mTOR via Akt and AMPK in the model of painful diabetic neuropathy (He et al., 2019). We speculate in this case that removal of APPL1 may be associated with disabling AMPK activity in the host cell, where the WT EEF is unable to effectively do so in the presence of *h*Rab5_Q79L-positive endosomes. Possibly the *Pb*Rab5b_Q91L mutant manages to restore this by outcompeting *h*Rab5_Q79L in capturing and sequestering APPL1 away from the host. The mechanistic details of the same remain an area for further investigation. In summary, we collectively link the removal of APPL1 from the host cytosol and retention on the PVM as a directed event to escape unfavorable host responses during *Plasmodium* exoerythrocytic infection.

Limitations of the study

Several questions remain open from this study, starting with the mechanism of *Pb*Rab5b access to the host cytosol. While there is a growing area of research focusing on unconventional mechanisms of *Plasmodium* protein export at the PVM, most of them are in *P. falciparum* blood stages, and are yet to be demonstrated in *P. berghei* liver stages. In this study we report that *Pb*Rab5b can be observed in the PVM/TVN but cannot comment on its orientation there. With increasing evidence of how phosphoinositides regulate assembly and disassembly of endosomal effectors (Kutateladze, 2010; Szentpetery et al., 2010; Zoncu et al., 2009), it is also of interest to test this for the PVM in liver-stage parasites. Presently, we lack the tools to alter local lipid composition in the PVM, restricting us to using small molecules to disrupt PVM protein delivery. Furthermore, the inability to knock out *Pb*Rab5b makes it complicated to assess the mechanism of APPL1 capture, transfer, and sequestration at the EEF. Unfortunately, conditional KD techniques for assessing liver-stage proteins throughout schizogony have not been effective or are incompatible with our study design. The attribution of APPL1 removal as necessary to rescue EEF size was derived correlatively from infection of *h*Rab5_Q79L-expressing cells with *Pb*Rab5b_Q91L parasites, which retained APPL1 at the

PVM and did not shrink in size like their WT counterparts. We cannot fully exclude other molecular components in this regard that may act in parallel or in sequence with APPL1 upon overexpression of *h*Rab5_Q79L mutant.

Furthermore, explorations of other host signaling adaptor proteins being manipulated during infection in hepatocytes may aid in shedding light on how the host is remodeled to alter the signaling landscape in favor of pathogen survival.

STAR★METHODS

Detailed methods are provided in the online version of this paper and include the following:

- KEY RESOURCES TABLE
- RESOURCE AVAILABILITY
  - Lead contact
  - Materials availability
  - Data and code availability
- EXPERIMENTAL MODEL AND SUBJECT DETAILS
  - Animal models
  - Mosquito rearing
  - Plasmodium parasite lines
  - Cell lines and primary cultures
- METHOD DETAILS
  - Molecular cloning
  - Plasmodium transfection
  - Cell culturing and transient transfection
  - Murine primary hepatocyte extraction and culturing *in vitro*
  - Sporozoite production
  - Stable transfection and cell line storage
  - Radiation inactivation of sporozoites
  - Mice infection and survival studies
  - *In vitro* sporozoites infection
  - Drug treatments in infected cells
  - Sample preparation for estimation of parasite burden
  - Mice transcardial perfusion
  - Murine liver cryosection
  - Murine liver floating section
  - Sample preparation for immunofluorescence assay and live fluorescence imaging
  - Microscopy
  - Structured illumination microscopy (SIM)
  - Sample processing for correlative light and electron microscopy (CLEM)
  - Workflow for correlative light and electron microscopy (CLEM)
  - Immunoprecipitation
  - SDS-PAGE and western blotting
- QUANTIFICATION AND STATISTICAL ANALYSIS
  - Statistical analysis
  - Image analysis

SUPPLEMENTAL INFORMATION

Supplemental information can be found online at https://doi.org/10.1016/j.celrep.2022.110886.

ACKNOWLEDGMENTS

From IMM-JLA, we thank Ana Parreira for *P. berghei*-infected *Anopheles* mosquito production and rearing, Viriato M'Bana and Carlos Almeida for help with mosquito/animal experiments and flow cytometry, Francisco Enguita for *Pb*Rab5b-related bioinformatics, Patricia Meireles and Miguel Prudêncio for guidance during lentiviral production/transduction, the bioimaging facility for assistance with microscopy, the rodent facility for the rederivation and maintenance of the APPL1 knockout mice line, and Helena Pinheiro for the artwork. We would like to express our gratitude to Miguel Prudêncio, Patricia Meireles, and João Mello-Vieira for the critical reading of this manuscript. We thank the Central Imaging and Flow Cytometry Facility (NCBS), Jana Meissner (Electron Microscopy Facility, MPI-CBG), and Sebastian Bundschuh (Light Microscopy Facility, MPI-CBG) for technical guidance and assistance. We are grateful to Yumiko Saito-Nakano and Izumi Taku (Department of Parasitology, National Institute of Infectious Diseases, Tokyo, Japan) for sharing the plasmids used to construct *P. berghei* lines expressing mAG-tagged *Pb*Rab5b WT and Q91L mutants and to the laboratories of Pietro de Camilli and Sergio Grinstein for gifting the plasmids for the expression of mRFP-APPL1 (#22202), mCherry-*h*Rab5-Q79L (#35138), and mCherry-*h*Rab5-S34N (#35139), respectively, through Addgene.

This work was supported by grants from the la Caixa Banking Foundation and Fundação para a Ciência e a Tecnologia (HR17-00264 and PTDC/SAU-PAR/30751/2017 respectively, both to M.M.M.). A.L and S.S.B were sponsored by Fundação para a Ciência e a Tecnologia fellowships (PD/BD/114036/2015, SFRH/BD/114464/2016, respectively). V.S acknowledges funding from the Science and Engineering Research Board (SERB) (EMR/2016/006810), Department of Science and Technology (DST), Government of India. V.P. and C.S. were supported by GRK2581 (P6) SPHINGOINF of the Growing Spine Foundation (DFG).

AUTHOR CONTRIBUTIONS

Conceptualization, A.L. and M.M.M.; investigation, A.L, S.S.B., S.M., V.P., V.Z.L., and V.S.; resources, C.S., M.Z., V.S., and M.M.M.; writing – original draft, A.L., S.M., and M.M.M.; review and editing, A.L., S.M., M.Z., V.S., and M.M.M.; supervision, V.Z.L., M.Z., and M.M.M.; funding acquisition, M.M.M.

DECLARATION OF INTERESTS

The authors declare no competing interests.

Received: October 6, 2021
Revised: January 10, 2022
Accepted: May 6, 2022
Published: May 31, 2022

REFERENCES

Agop-Nersesian, C., De Niz, M., Niklaus, L., Prado, M., Eickel, N., and Heussler, V.T. (2017). Shedding of host autophagic proteins from the parasitophorous vacuolar membrane of Plasmodium berghei. Sci. Rep. *7*, 2191. https://doi.org/10.1038/s41598-017-02156-7.

Amos, B., Aurrecoechea, C., Barba, M., Barreto, A., Basenko, E.Y., Bażant, W., Belnap, R., Blevins, A.S., Böhme, U., Brestelli, J., et al. (2022). VEuPathDB: the eukaryotic pathogen, vector and host bioinformatics resource center. Nucleic Acids Res. *50*, D898–D911.

Banach-Orlowska, M., Pilecka, I., Torun, A., Pyrzynska, B., and Miaczynska, M. (2009). Functional characterization of the interactions between endosomal adaptor protein APPL1 and the NuRD co-repressor complex. Biochem. J. *423*, 389–400. https://doi.org/10.1042/bj20090086.

Bano, N., Romano, J.D., Jayabalasingham, B., and Coppens, I. (2007). Cellular interactions of Plasmodium liver stage with its host mammalian cell. Int. J. Parasitol. *37*, 1329–1341. https://doi.org/10.1016/j.ijpara.2007.04.005.

Bohdanowicz, M., Balkin, D.M., De Camilli, P., and Grinstein, S. (2011). Recruitment of OCRL and Inpp5B to phagosomes by Rab5 and APPL1

depletes phosphoinositides and attenuates Akt signaling. Mol. Biol. Cell *23*, 176–187. https://doi.org/10.1091/mbc.e11-06-0489.

Brumell, J.H., and Scidmore, M.A. (2007). Manipulation of rab GTPase function by intracellular bacterial pathogens. Microbiol. Mol. Biol. Rev. *71*, 636–652. https://doi.org/10.1128/mmbr.00023-07.

Bucci, C., Wandinger-Ness, A., Lütcke, A., Chiariello, M., Bruni, C.B., and Zerial, M. (1994). Rab5a is a common component of the apical and basolateral endocytic machinery in polarized epithelial cells. Proc. Natl. Acad. Sci. U S A *91*, 5061–5065. https://doi.org/10.1073/pnas.91.11.5061.

Cheng, K.K.Y., Lam, K.S.L., Wang, Y., Huang, Y., Carling, D., Wu, D., Wong, C., and Xu, A. (2007). Adiponectin-induced endothelial nitric oxide synthase activation and nitric oxide production are mediated by APPL1 in endothelial cells. Diabetes *56*, 1387–1394. https://doi.org/10.2337/db06-1580.

Dadson, K., Chasiotis, H., Wannaiampikul, S., Tungtrongchitr, R., Xu, A., and Sweeney, G. (2014). Adiponectin mediated APPL1-AMPK signaling induces cell migration, MMP activation, and collagen remodeling in cardiac fibroblasts. J. Cell Biochem. *115*, 785–793. https://doi.org/10.1002/jcb.24722.

De Niz, M., Kaiser, G., Zuber, B., Heo, W.D., Heussler, V.T., and Nersesian, C.A. (2020). Hijacking of the host cell Golgi by Plasmodium liver stage parasites. Preprint at bioRxiv. https://doi.org/10.1101/2020.07.24.220137.

Denny, P.W., Gokool, S., Russell, D.G., Field, M.C., and Smith, D.F. (2000). Acylation-dependent protein export inLeishmania. J. Biol. Chem. *275*, 11017–11025. https://doi.org/10.1074/jbc.275.15.11017.

Deschermeier, C., Hecht, L.-S., Bach, F., Rützel, K., Stanway, R.R., Nagel, A., Seeber, F., and Heussler, V.T. (2012). Mitochondrial lipoic acid scavenging is essential for Plasmodium berghei liver stage development. Cell Microbiol. *14*, 416–430. https://doi.org/10.1111/j.1462-5822.2011.01729.x.

Dokainish, H., Gavicherla, B., Shen, Y., and Ireton, K. (2007). The carboxyl-terminal SH3 domain of the mammalian adaptor CrkII promotes internalization of Listeria monocytogenes through activation of host phosphoinositide 3-kinase. Cell Microbiol. *9*, 2497–2516. https://doi.org/10.1111/j.1462-5822.2007.00976.x.

Ebine, K., Hirai, M., Sakaguchi, M., Yahata, K., Kaneko, O., and Saito-Nakano, Y. (2016). Plasmodium Rab5b is secreted to the cytoplasmic face of the tubovesicular network in infected red blood cells together with N-acylated adenylate kinase 2. Malar. J. *15*, 323. https://doi.org/10.1186/s12936-016-1377-4.

Erdmann, K.S., Mao, Y., McCrea, H.J., Zoncu, R., Lee, S., Paradise, S., Modregger, J., Biemesderfer, D., Toomre, D., and De Camilli, P. (2007). A role of the Lowe syndrome protein OCRL in early steps of the endocytic pathway. Dev Cell. *13*, 377–390.

Ezougou, C.N., Ben-Rached, F., Moss, D.K., Lin, J.w., Black, S., Knuepfer, E., Green, J.L., Khan, S.M., Mukhopadhyay, A., Janse, C.J., et al. (2014). Plasmodium falciparum Rab5B is an N-terminally myristoylated rab GTPase that is targeted to the parasite's plasma and food vacuole membranes. PLoS One *9*, e87695. https://doi.org/10.1371/journal.pone.0087695.

Fougère, A., Jackson, A.P., Paraskevi Bechtsi, D., Braks, J.A.M., Annoura, T., Fonager, J., Spaccapelo, R., Ramesar, J., Chevalley-Maurel, S., Klop, O., et al. (2016). Variant exported blood-stage proteins encoded by plasmodium multigene Families are expressed in liver stages where they are exported into the parasitophorous vacuole. PLoS Pathog. *12*, e1005917. https://doi.org/10.1371/journal.ppat.1005917.

Gage, G.J., Kipke, D.R., and Shain, W. (2012). Whole animal perfusion fixation for rodents. JoVE *30*, 3564. https://doi.org/10.3791/3564.

Glennon, E.K.K., Austin, L.S., Arang, N., Kain, H.S., Mast, F.D., Vijayan, K., Aitchison, J.D., Kappe, S.H.I., and Kaushansky, A. (2019). Alterations in phosphorylation of hepatocyte ribosomal protein S6 control plasmodium liver stage infection. Cell Rep. *26*, 3391–3399.e4. https://doi.org/10.1016/j.celrep.2019.02.085.

Goto-Silva, L., McShane, M.P., Salinas, S., Kalaidzidis, Y., Schiavo, G., and Zerial, M. (2019). Retrograde transport of Akt by a neuronal Rab5-APPL1 endosome. Sci. Rep. *9*, 2433. https://doi.org/10.1038/s41598-019-38637-0.

Grabinski, T., and Kanaan, N.M. (2016). Novel non-phosphorylated serine 9/21 GSK3β/α antibodies: expanding the tools for studying GSK3 regulation. Front. Mol. Neurosci. *9*, 123. https://doi.org/10.3389/fnmol.2016.00123.

Grützke, J., Rindte, K., Goosmann, C., Silvie, O., Rauch, C., Heuer, D., Lehmann, M.J., Mueller, A.-K., Brinkmann, V., Matuschewski, K., and Ingmundson, A. (2014). The spatiotemporal dynamics and membranous features of the plasmodium liver stage tubovesicular network. Traffic *15*, 362–382. https://doi.org/10.1111/tra.12151.

Hanson, K.K., Ressurreição, A.S., Buchholz, K., Prudêncio, M., Herman-Ornelas, J.D., Rebelo, M., Beatty, W.L., Wirth, D.F., Hänscheid, T., Moreira, R., et al. (2013). Torins are potent antimalarials that block replenishment of Plasmodium liver stage parasitophorous vacuole membrane proteins. Proc. Natl. Acad. Sci. U S A *110*, E2838–E2847. https://doi.org/10.1073/pnas.1306097110.

He, W.-Y., Zhang, B., Zhao, W.-C., He, J., Wang, Y., Zhang, L., Xiong, Q.-M., and Wang, H.-B. (2019). mTOR activation due to APPL1 deficiency exacerbates hyperalgesia via Rab5/Akt and AMPK signaling pathway in streptozocin-induced diabetic rats. Mol. Pain *15*, 174480691988064. https://doi.org/10.1177/1744806919880643.

Hiller, N.L., Bhattacharjee, S., van Ooij, C., Liolios, K., Harrison, T., Lopez-Estraño, C., and Haldar, K. (2004). A host-targeting signal in virulence proteins reveals a secretome in malarial infection. Science *306*, 1934–1937. https://doi.org/10.1126/science.1102737.

Huff, J. (2016). The Fast mode for ZEISS LSM 880 with Airyscan: high-speed confocal imaging with super-resolution and improved signal-to-noise ratio. Nat. Methods *13*, i–ii. https://doi.org/10.1038/nmeth.f.398.

Itoe, M.A., Sampaio, J.L., Cabal, G.G., Real, E., Zuzarte-Luis, V., March, S., Bhatia, S.N., Frischknecht, F., Thiele, C., Shevchenko, A., and Mota, M. (2014). Host cell phosphatidylcholine is a key mediator of malaria parasite survival during liver stage infection. Cell Host Microbe. *16*, 778–786. https://doi.org/10.1016/j.chom.2014.11.006.

Janse, C.J., Ramesar, J., and Waters, A.P. (2006). High-efficiency transfection and drug selection of genetically transformed blood stages of the rodent malaria parasite Plasmodium berghei. Nat. Protoc. *1*, 346–356. https://doi.org/10.1038/nprot.2006.53.

Kalaidzidis, I., Miaczynska, M., Brewińska-Olchowik, M., Hupalowska, A., Ferguson, C., Parton, R.G., Kalaidzidis, Y., and Zerial, M. (2015). APPL endosomes are not obligatory endocytic intermediates but act as stable cargo-sorting compartments. J. Cell Biol. *211*, 123–144. https://doi.org/10.1083/jcb.201311117.

Kaushansky, A., Ye, A.S., Austin, L.S., Mikolajczak, S.A., Vaughan, A.M., Camargo, N., Metzger, P.G., Douglass, A.N., MacBeath, G., and Kappe, S.H.I. (2013). Suppression of host p53 is critical for plasmodium liver-stage infection. Cell Rep. *3*, 630–637. https://doi.org/10.1016/j.celrep.2013.02.010.

King, G.J., Stöckli, J., Hu, S.-H., Winnen, B., Duprez, W.G.A., Meoli, C.C., Junutula, J.R., Jarrott, R.J., James, D.E., Whitten, A.E., and Martin, J.L. (2012). Membrane curvature protein exhibits interdomain Flexibility and binds a small GTPase. J. Biol. Chem. *287*, 40996–41006. https://doi.org/10.1074/jbc.m112.349803.

Krishnan, K., Ziniel, P., Li, H., Huang, X., Hupalo, D., Gombakomba, N., Guerrero, S.M., Dotrang, T., Lu, X., Caridha, D., et al. (2020). Torin 2 derivative, NCATS-SM3710, has potent multistage antimalarial activity through inhibition of P. Falciparum phosphatidylinositol 4-kinase (pf PI4KIIIβ). ACS Pharmacol. Transl. Sci. *3*, 948–964. https://doi.org/10.1021/acsptsci.0c00078.

Kutateladze, T.G. (2010). Translation of the phosphoinositide code by PI effectors. Nat. Chem. Biol. *6*, 507–513. https://doi.org/10.1038/nchembio.390.

Labaied, M., Jayabalasingham, B., Bano, N., Cha, S.-J., Sandoval, J., Guan, G., and Coppens, I. (2011). Plasmodium salvages cholesterol internalized by LDL and synthesized de novo in the liver. Cell Microbiol. *13*, 569–586. https://doi.org/10.1111/j.1462-5822.2010.01555.x.

Leirião, P., Albuquerque, S.S., Corso, S., Van Gemert, G.J., Sauerwein, R.W., Rodriguez, A., Giordano, S., and Mota, M.M. (2005). HGF/MET signalling protects Plasmodium-infected host cells from apoptosis. Cell Microbiol. *7*, 603–609. https://doi.org/10.1111/j.1462-5822.2004.00490.x.

Lin, J.W., Annoura, T., Sajid, M., Chevalley-Maurel, S., Ramesar, J., Klop, O., Franke-Fayard, B.M.D., Janse, C.J., and Khan, S.M. (2011). A novel 'gene insertion/marker out' (GIMO) method for transgene expression and gene complementation in rodent malaria parasites. PLoS One. *6*, e29289.

Liu, Q., Kang, S.A., Thoreen, C.C., Hur, W., Wang, J., Chang, J.W., Markhard, A., Zhang, J., Sim, T., Sabatini, D.M., and Gray, N.S. (2012). Development of ATP-competitive mTOR inhibitors. Methods Mol. Biol. *821*, 447–460. https://doi.org/10.1007/978-1-61779-430-8_29.

Liu, Q., Xu, C., Kirubakaran, S., Zhang, X., Hur, W., Liu, Y., Kwiatkowski, N.P., Wang, J., Westover, K.D., Gao, P., et al. (2013). Characterization of Torin2, an ATP-competitive inhibitor of mTOR, ATM and ATR. Cancer Res. *73*, 2574–2586. https://doi.org/10.1158/0008-5472.can-12-1702.

Lopes da Silva, M., Thieleke-Matos, C., Cabrita-Santos, L., Ramalho, J.S., Wavre-Shapton, S.T., Futter, C.E., Barral, D.C., and Seabra, M.C. (2012). The host endocytic pathway is essential for plasmodium berghei late liver stage development. Traffic *13*, 1351–1363. https://doi.org/10.1111/j.1600-0854.2012.01398.x.

Mao, X., Kikani, C.K., Riojas, R.A., Langlais, P., Wang, L., Ramos, F.J., Fang, Q., Christ-Roberts, C.Y., Hong, J.Y., Kim, R.-Y., et al. (2006). APPL1 binds to adiponectin receptors and mediates adiponectin signalling and function. Nat. Cell Biol. *8*, 516–523. https://doi.org/10.1038/ncb1404.

Markert, S.M., Britz, S., Proppert, S., Lang, M., Witvliet, D., Mulcahy, B., Sauer, M., Zhen, M., Bessereau, J.-L., and Stigloher, C. (2016). Filling the gap: adding super-resolution to array tomography for correlated ultrastructural and molecular identification of electrical synapses at the C. elegans connectome. Neurophotonics *3*, 041802. https://doi.org/10.1117/1.nph.3.4.041802.

Markert, S.M., Bauer, V., Muenz, T.S., Jones, N.G., Helmprobst, F., Britz, S., Sauer, M., Rössler, W., Engstler, M., and Stigloher, C. (2017). Chapter 2 - 3D subcellular localization with superresolution array tomography on ultrathin sections of various species. In Methods in Cell Biology, T. Müller-Reichert and P. Verkade, eds. (Academic Press), pp. 21–47.

Marti, M., Good, R.T., Rug, M., Knuepfer, E., and Cowman, A.F. (2004). Targeting malaria virulence and remodeling proteins to the host erythrocyte. Science *306*, 1930–1933. https://doi.org/10.1126/science.1102452.

Martinez-Quiles, N., Feuerbacher, L.A., Benito-León, M., and Hardwidge, P.R. (2014). Contribution of Crk Adaptor Proteins to Host Cell and Bacteria Interactions (Hindawi)).

M'Bana, V., Lahree, A., Marques, S., Slavic, K., and Mota, M.M. (2021). *Plasmodium* Parasitophorous Vacuole Membrane-Resident Protein UIS4 Manipulates Host Cell Actin to Avoid Parasite Elimination (Social Science Research Network).

McNamara, C.W., Lee, M.C., Lim, C.S., Lim, S.H., Roland, J., Simon, O., Yeung, B.K., Chatterjee, A.K., McCormack, S.L., Manary, M.J., et al. (2013). Targeting Plasmodium PI(4)K to eliminate malaria. Nature *504*, 248–253. https://doi.org/10.1038/nature12782.

Meireles, P., Sales-Dias, J., Andrade, C.M., Mello-Vieira, J., Mancio-Silva, L., Simas, J.P., Staines, H.M., and Prudêncio, M. (2017). GLUT1-mediated glucose uptake plays a crucial role during Plasmodium hepatic infection. Cell Microbiol. *19*, e12646. https://doi.org/10.1111/cmi.12646.

Miaczynska, M., Christoforidis, S., Giner, A., Shevchenko, A., Uttenweiler-Joseph, S., Habermann, B., Wilm, M., Parton, R.G., and Zerial, M. (2004). APPL proteins link Rab5 to nuclear signal transduction via an endosomal compartment. Cell *116*, 445–456. https://doi.org/10.1016/s0092-8674(04)00117-5.

Möskes, C., Burghaus, P.A., Wernli, B., Sauder, U., Dürrenberger, M., and Kappes, B. (2004). Export of Plasmodium falciparum calcium-dependent protein kinase 1 to the parasitophorous vacuole is dependent on three N-terminal membrane anchor motifs. Mol. Microbiol. *54*, 676–691. https://doi.org/10.1111/j.1365-2958.2004.04313.x.

Murphy, J.E., Padilla, B.E., Hasdemir, B., Cottrell, G.S., and Bunnett, N.W. (2009). Endosomes: a legitimate platform for the signaling train. Proc. Natl. Acad. Sci. U S A *106*, 17615–17622. https://doi.org/10.1073/pnas.0906541106.

Petersen, W., Stenzel, W., Silvie, O., Blanz, J., Saftig, P., Matuschewski, K., and Ingmundson, A. (2017). Sequestration of cholesterol within the host late endocytic pathway restricts liver-stage Plasmodium development. Mol. Biol. Cell *28*, 726–735. https://doi.org/10.1091/mbc.e16-07-0531.

Pielage, J.F., Powell, K.R., Kalman, D., and Engel, J.N. (2008). RNAi screen reveals an abl kinase-dependent host cell pathway involved in Pseudomonas aeruginosa internalization. PLoS Pathog. *4*, e1000031. https://doi.org/10.1371/journal.ppat.1000031.

Posfai, D., Sylvester, K., Reddy, A., Ganley, J.G., Wirth, J., Cullen, Q.E., Dave, T., Kato, N., Dave, S.S., and Derbyshire, E.R. (2018). Plasmodium parasite exploits host aquaporin-3 during liver stage malaria infection. PLoS Pathog. *14*, e1007057. https://doi.org/10.1371/journal.ppat.1007057.

Prieto, D., Aparicio, G., Machado, M., and Zolessi, F.R. (2015). Application of the DNA-specific stain methyl green in the fluorescent labeling of embryos. J. Vis. Exp. *99*, 52769. https://doi.org/10.3791/52769.

Quevillon, E., Spielmann, T., Brahimi, K., Chattopadhyay, D., Yeramian, E., and Langsley, G. (2003). The Plasmodium falciparum family of Rab GTPases. Gene *306*, 13–25. https://doi.org/10.1016/s0378-1119(03)00381-0.

Rashid, S., Pilecka, I., Torun, A., Olchowik, M., Bielinska, B., and Miaczynska, M. (2009). Endosomal adaptor proteins APPL1 and APPL2 are novel activators of β-Catenin/TCF-mediated transcription. J. Biol. Chem. *284*, 18115–18128. https://doi.org/10.1074/jbc.m109.007237.

Real, E., Rodrigues, L., Cabal, G.G., Enguita, F.J., Mancio-Silva, L., Mello-Vieira, J., Beatty, W., Vera, I.M., Zuzarte-Luís, V., Figueira, T.N., et al. (2018). Plasmodium UIS3 sequesters host LC3 to avoid elimination by autophagy in hepatocytes. Nat. Microbiol. *3*, 17–25. https://doi.org/10.1038/s41564-017-0054-x.

Ridzuan, M.A.M., Moon, R.W., Knuepfer, E., Black, S., Holder, A.A., and Green, J.L. (2012). Subcellular location, phosphorylation and assembly into the motor complex of GAP45 during plasmodium falciparum schizont development. PLoS One *7*, e33845. https://doi.org/10.1371/journal.pone.0033845.

Romano, J.D., Nolan, S.J., Porter, C., Ehrenman, K., Hartman, E.J., Hsia, R., and Coppens, I. (2017). The parasite Toxoplasma sequesters diverse Rab host vesicles within an intravacuolar network. J. Cell Biol. *216*, 4235–4254. https://doi.org/10.1083/jcb.201701108.

Ruivo, M.T.G., Vera, I.M., Sales-Dias, J., Meireles, P., Gural, N., Bhatia, S.N., Mota, M.M., and Mancio-Silva, L. (2016). Host AMPK is a modulator of plasmodium liver infection. Cell Rep. *16*, 2539–2545. https://doi.org/10.1016/j.celrep.2016.08.001.

Ryu, J., Galan, A.K., Xin, X., Dong, F., Abdul-Ghani, M.A., Zhou, L., Wang, C., Li, C., Holmes, B.M., Sloane, L.B., et al. (2014). APPL1 potentiates insulin sensitivity by facilitating the binding of IRS1/2 to the insulin receptor. Cell Rep. *7*, 1227–1238. https://doi.org/10.1016/j.celrep.2014.04.006.

Sá E Cunha, C., Nyboer, B., Heiss, K., Sanches-Vaz, M., Fontinha, D., Wiedtke, E., Grimm, D., Przyborski, J.M., Mota, M.M., Prudêncio, M., and Mueller, A.K. (2017). Plasmodium berghei EXP-1 interacts with host Apolipoprotein H during Plasmodium liver-stage development. Proc. Natl. Acad. Sci. U S A *114*, E1138–E1147. https://doi.org/10.1073/pnas.1606419114.

van de Sand, C., Horstmann, S., Schmidt, A., Sturm, A., Bolte, S., Krueger, A., Lütgehetmann, M., Pollok, J.-M., Libert, C., and Heussler, V.T. (2005). The liver stage of Plasmodium berghei inhibits host cell apoptosis. Mol. Microbiol. *58*, 731–742. https://doi.org/10.1111/j.1365-2958.2005.04888.x.

Sayeed, M., Gautam, S., Verma, D.P., Afshan, T., Kumari, T., Srivastava, A.K., and Ghosh, J.K. (2018). A collagen domain–derived short adiponectin peptide activates APPL1 and AMPK signaling pathways and improves glucose and fatty acid metabolisms. J. Biol. Chem. *293*, 13509–13523. https://doi.org/10.1074/jbc.ra118.001801.

Schenck, A., Goto-Silva, L., Collinet, C., Rhinn, M., Giner, A., Habermann, B., Brand, M., and Zerial, M. (2008). The endosomal protein Appl1 mediates Akt substrate specificity and cell survival in vertebrate development. Cell *133*, 486–497. https://doi.org/10.1016/j.cell.2008.02.044.

Schindelin, J., Arganda-Carreras, I., Frise, E., Kaynig, V., Longair, M., Pietzsch, T., Preibisch, S., Rueden, C., Saalfeld, S., Schmid, B., et al. (2012). Fiji: an

open-source platform for biological-image analysis. Nat. Methods *9*, 676–682. https://doi.org/10.1038/nmeth.2019.

Schulze, R.J., Schott, M.B., Casey, C.A., Tuma, P.L., and McNiven, M.A. (2019). The cell biology of the hepatocyte: a membrane trafficking machine. J. Cell Biol. *218*, 2096–2112. https://doi.org/10.1083/jcb.201903090.

Setua, S., Enguita, F.J., Chora, Â.F., Ranga-Prasad, H., Lahree, A., Marques, S., Sundaramurthy, V., and Mota, M.M. (2020). Disrupting Plasmodium UIS3-host LC3 interaction with a small molecule causes parasite elimination from host cells. Commun. Biol. *3*, 688. https://doi.org/10.1038/s42003-020-01422-1.

Sigismund, S., Confalonieri, S., Ciliberto, A., Polo, S., Scita, G., and Di Fiore, P.P. (2012). Endocytosis and signaling: cell logistics shape the eukaryotic cell plan. Physiol. Rev. *92*, 273–366. https://doi.org/10.1152/physrev.00005.2011.

Sigler, C.I., Leland, P., and Hollingdale, M.R. (1984). In vitro infectivity of irradiated Plasmodium berghei sporozoites to cultured hepatoma cells. Am. J. Trop. Med. Hyg. *33*, 544–547. https://doi.org/10.4269/ajtmh.1984.33.544.

Sinz, A. (2010). Investigation of protein-protein interactions in living cells by chemical crosslinking and mass spectrometry. Anal Bioanal. Chem. *397*, 3433–3440. https://doi.org/10.1007/s00216-009-3405-5.

Slavic, K., Krishna, S., Lahree, A., Bouyer, G., Hanson, K.K., Vera, I., Pittman, J.K., Staines, H.M., and Mota, M.M. (2016). A vacuolar iron-transporter homologue acts as a detoxifier in Plasmodium. Nat commun. *7*, 10403.

Stenmark, H., Parton, R.G., Steele-Mortimer, O., Lütcke, A., Gruenberg, J., and Zerial, M. (1994). Inhibition of rab5 GTPase activity stimulates membrane fusion in endocytosis. EMBO J. *13*, 1287–1296. https://doi.org/10.1002/j.1460-2075.1994.tb06381.x.

Szentpetery, Z., Várnai, P., and Balla, T. (2010). Acute manipulation of Golgi phosphoinositides to assess their importance in cellular trafficking and signaling. Proc. Natl. Acad. Sci. U S A *107*, 8225–8230. https://doi.org/10.1073/pnas.1000157107.

Taku, I., Hirai, T., Makiuchi, T., Shinzawa, N., Iwanaga, S., Annoura, T., Nagamune, K., Nozaki, T., and Saito-Nakano, Y. (2021). Rab5b-Associated Arf1 GTPase regulates export of N-myristoylated adenylate kinase 2 from the endoplasmic reticulum in plasmodium falciparum. Front. Cell. Infect. Microbiol. *10*, 610200. https://doi.org/10.3389/fcimb.2020.610200.

Tan, Y., You, H., Wu, C., Altomare, D.A., and Testa, J.R. (2010). Appl1 is dispensable for mouse development, and loss of Appl1 has growth factor-selective effects on Akt signaling in murine embryonic fibroblasts. J. Biol. Chem. *285*, 6377–6389. https://doi.org/10.1074/jbc.m109.068452.

Thavayogarajah, T., Gangopadhyay, P., Rahlfs, S., Becker, K., Lingelbach, K., Przyborski, J.M., and Holder, A.A. (2015). Alternative protein secretion in the malaria parasite plasmodium falciparum. PLoS One *10*, e0125191. https://doi.org/10.1371/journal.pone.0125191.

Thieleke-Matos, C., Lopes da Silva, M., Cabrita-Santos, L., Portal, M.D., Rodrigues, I.P., Zuzarte-Luis, V., Ramalho, J.S., Futter, C.E., Mota, M.M., Barral, D.C., and Seabra, M.C. (2016). Host cell autophagy contributes to Plasmodium liver development. Cell Microbiol. *18*, 437–450. https://doi.org/10.1111/cmi.12524.

Tsuji, M., Mattei, D., Nussenzweig, R.S., Eichinger, D., and Zavala, F. (1994). Demonstration of heat-shock protein 70 in the sporozoite stage of malaria parasites. Parasitol. Res. *80*, 16–21. https://doi.org/10.1007/bf00932618.

Ueda, T., Yamaguchi, M., Uchimiya, H., and Nakano, A. (2001). Ara6, a plant-unique novel type Rab GTPase, functions in the endocytic pathway of Arabidopsis thaliana. EMBO J. *20*, 4730–4741. https://doi.org/10.1093/emboj/20.17.4730.

Vijayan, K., Arang, N., Wei, L., Morrison, R., Geiger, R., Parks, K.R., Lewis, A.J., Mast, F.D., Douglass, A.N., Kain, H.S., et al. (2020). A genome-wide CRISPR-cas9 screen identifies host factors essential for optimal plasmodium liver stage development. Preprint at bioRxiv. https://doi.org/10.1101/2020.08.31.275867.

Villaseñor, R., Kalaidzidis, Y., and Zerial, M. (2016). Signal processing by the endosomal system. Curr. Opin. Cell Biol. *39*, 53–60. https://doi.org/10.1016/j.ceb.2016.02.002.

Wang, L., and Boyer, J.L. (2004). The maintenance and generation of membrane polarity in hepatocytes. Hepatology *39*, 892–899. https://doi.org/10.1002/hep.20039.

Wang, M., and Casey, P.J. (2016). Protein prenylation: unique fats make their mark on biology. Nat. Rev. Mol. Cell Biol. *17*, 110–122. https://doi.org/10.1038/nrm.2015.11.

Ward, G.E., Tilney, L.G., and Langsley, G. (1997). Rab GTPases and the unusual secretory pathway of plasmodium. Parasitol. Today *13*, 57–62. https://doi.org/10.1016/s0169-4758(96)10080-6.

Yuan, M., Deleuil, F., and Fällman, M. (2005). Interaction between the *Yersinia* tyrosine phosphatase YopH and its macrophage substrate, Fyn-binding protein, Fyb. J. Mol. Microbiol. Biotechnol. *9*, 214–223. https://doi.org/10.1159/000089649.

Zeigerer, A., Bogorad, R.L., Sharma, K., Gilleron, J., Seifert, S., Sales, S., Berndt, N., Bulik, S., Marsico, G., D'Souza, R.C.J., et al. (2015). Regulation of liver metabolism by the endosomal GTPase Rab5. Cell Rep. *11*, 884–892. https://doi.org/10.1016/j.celrep.2015.04.018.

Zhou, L., Deepa, S.S., Etzler, J.C., Ryu, J., Mao, X., Fang, Q., Liu, D.D., Torres, J.M., Jia, W., Lechleiter, J.D., et al. (2009). Adiponectin activates AMP-activated protein kinase in muscle cells via APPL1/LKB1-dependent and phospholipase C/Ca2+/Ca2+/Calmodulin-dependent protein kinase kinase-dependent pathways. J. Biol. Chem. *284*, 22426–22435. https://doi.org/10.1074/jbc.m109.028357.

Zhu, G., Chen, J., Liu, J., Brunzelle, J.S., Huang, B., Wakeham, N., Terzyan, S., Li, X., Rao, Z., Li, G., and Zhang, X.C. (2007). Structure of the APPL1 BAR-PH domain and characterization of its interaction with Rab5. EMBO J. *26*, 3484–3493. https://doi.org/10.1038/sj.emboj.7601771.

Zoncu, R., Perera, R.M., Balkin, D.M., Pirruccello, M., Toomre, D., and De Camilli, P. (2009). A phosphoinositide switch controls the maturation and signaling properties of APPL endosomes. Cell *136*, 1110–1121. https://doi.org/10.1016/j.cell.2009.01.032.

STAR★METHODS

KEY RESOURCES TABLE

REAGENT or RESOURCE	SOURCE	IDENTIFIER
Antibodies		
Polyclonal a goat α UIS4	SICGEN	Cat# AB0042; RRID: AB_2333159
Polyclonal rabbit α APPL1	Merck Millipore	Cat# ABS314
Polyclonal rabbit α APPL1	(Miaczynska et al., 2004)	N/A
Polyclonal rabbit α monomeric Azami-green	MBL International Corporation	Cat# PM052M, RRID: AB_2827721
Polyclonal rabbit α Rab5	(Bucci et al., 1994)	N/A
Monoclonal rat anti-tyrosinated-α-tubulin (clone YL1/2)	Gift from Edgar Gomes	Cat#92092402; RRID: CVCL_J781
Monoclonal rat α HA (clone 3F10)	Roche	Cat# 1867423001, RRID: AB_390918
Alexa-488 dye conjugated donkey α goat IgG	Thermo Fisher Scientific	Cat# A32814, RRID: AB_2762838
Alexa-647 dye conjugated donkey α rabbit IgG	Thermo Fisher Scientific	Cat# A32795, RRID: AB_2762835
DyLight 594 dye conjugated donkey α rat IgG	Invitrogen Thermo Fisher Scientific	Cat# SA5-10028, RRID: AB_2556608
Alexa-555 dye conjugated donkey α mouse IgG	Invitrogen Thermo Fisher Scientific	Cat# A32773, RRID: AB_2762848
Alexa-555 conjugated Phalloidin	Invitrogen	Cat# A34055
Hoechst 33342	Invitrogen	Cat# H1399
Monoclonal rabbit α HA (clone C29F4)	Cell Signaling Technology	Cat# 3724S, RRID: AB_1549585
Polyclonal rabbit α mCherry	Abcam	Cat# ab167453, RRID: AB_2571870
Rabbit α phospho-Akt (S473)	Cell Signaling Technology	Cat# 9271, RRID: AB_329825
Rabbit α phospho-GSK-3β (S9)	Cell Signaling Technology	Cat# 5558, RRID: AB_10013750
Rabbit α phospho-AMPK (T172)	Cell Signaling Technology	Cat# 2535, RRID: AB_331250
Rabbit α total Akt	Cell Signaling Technology	Cat# 9272, RRID: AB_329827
Rabbit α total GSK-3β	Cell Signaling Technology	Cat# 12456, RRID: AB_2636978
Rabbit α total AMPK	Cell Signaling Technology	Cat# 2603, RRID: AB_490795
Mouse α beta-actin	Abcam	Cat# ab8224, RRID: AB_449644
Goat α mouse IgG F(ab')2, polyclonal antibody HRP conjugate	Enzo Life Sciences	Cat# BML-SA204-0100, RRID: AB_2051534
Goat α rabbit IgG, HRP-linked Antibody	Cell Signaling Technology	Cat# 7074, RRID: AB_2099233
Mouse α rabbit IgG HRP-linked Antibody	Rockland Immunochemicals, Inc	Cat# 18-8816-31, RRID: AB_2610847
Rat α mouse IgG HRP-linked Antibody	Rockland Immunochemicals, Inc	Cat# 18-8817-30, RRID: AB_2610849
Polyclonal rabbit α APPL2	Sigma Aldrich	Cat# HPA039688, RRID: AB_2676626
Rabbit α goat IgG HRP-linked Antibody	Thermo Fisher Scientific	Cat# 81-1620, RRID: AB_2534006
Alexa Fluor® 594 AffiniPure Goat Anti-Rabbit IgG (H+L)	Jackson Immunoresearch	Cat#111-585-144, RRID: AB_2307325
Alexa Fluor® 488 AffiniPure Donkey Anti-Goat IgG (H + L)	Jackson Immunoresearch	Cat# 705-545-003, RRID: AB_2340428
Giemsa stain, Modified Solution	Sigma Aldrich	Cat# 48900
Trypan Blue solution	Sigma Aldrich	Cat# T8154
Bacterial and virus strains		
E. coli BL21(DE3)	Nzytech	Cat#MB006
Competent cell _ XL10-Gold Ultracompetent Cells	Agilent	Cat# 200315
Δ8.9 and VSV-G lentiviral expression vectors	(Meireles et al., 2017)	N/A
Biological samples		
C57Bl/6J Mouse Liver	This study	N/A
C57Bl/6J Mouse Blood	This study	N/A
BALB/cJ Mouse Blood	This study	N/A

(*Continued on next page*)

Continued

REAGENT or RESOURCE	SOURCE	IDENTIFIER
Chemicals, peptides, and recombinant proteins		
KDU-691	Sigma Aldrich	Cat#SML2375
Cytochalasin D	Merck	Cat# C8273
Nocodazole	Sigma Aldrich	Cat# M1404
Paraformaldehyde 4% (PFA)	ChemCruz	Cat# sc-281692
Triton X-100	Sigma	Cat# 9002-93-1
Amphotericin B (Fungizone)	Gibco	Cat#15290018
Ampicillin	Sigma Aldrich	Cat#A9393
Gentamicin	Gibco	Cat#15750-037
Pyrimethamine	Sigma Aldrich	Cat# P7771
Puromycin dihydrochloride	Sigma Aldrich	Cat# P8833
Phusion™ High-Fidelity DNA Polymerase (2 U/μL)	Thermo Scientific	Cat# F530S
HindIII-HF	New England Bioloabs	Cat# R3104S
NotI-HF	New England Bioloabs	Cat# R3189S
KpnI	New England Bioloabs	Cat# R0142S
EcoRI-HF	New England Bioloabs	Cat# R3101S
T4 DNA Ligase	New England Bioloabs	Cat# M0202S
Fluoromount-G	Thermo fisher	Cat# 00-4958-02
Nycodenz	Axis-Shield	Cat# 1002424
O.C.T. Compound	Sakura Finetek	Cat# 4583
Collagen, Type I solution from rat tail	Sigma Aldrich	Cat# C3867
Glutaraldehyde solution	Sigma Aldrich	Cat# G5882
Dimethyl sulfoxide (DMSO)	Sigma Aldrich	Cat# D2650
Liver Perfusion Medium (1X)	Gibco	Cat# 11540536
Liver Digest Medium	Gibco	Cat# 11550536
Fugene 6 Transfection reagent	Promega	Cat# PROME2691
Percoll	Sigma Aldrich	Cat# P4937
William's E Medium, GlutaMAX™ Supplement	Gibco	Cat# 11514466
DMEM- high glucose, HEPES, no phenol red	Gibco	Cat# 21063-029
Opti-MEM™ I Reduced Serum Medium, no phenol red	Gibco	Cat# 11058-021
Critical commercial assays		
QIAquick Gel Extraction Kit	Qiagen	Cat# 28706X4
QIAquick PCR Purification Kit	Qiagen	Cat# 28104
Protein quantification: Pierce™ BCA Protein Assay Kit	Thermo Scientific	Cat#23227
NZY Blood gDNA Isolation kit	Nzytech	Cat# MB13602
RNA extraction kit	Nzytech	Cat# MB13402
CloneJET PCR Cloning Kit	Thermo Scientific	Cat# K1231
NZY Tissue gDNA Isolation kit	Nzytech	Cat# MB135
NZY Miniprep	Nzytech	Cat# MB010
Experimental models: Cell lines		
C57Bl/6J primary hepatocytes	This study	N/A
Human Hepatoma Cell line_HepG2 cell line	ATCC	Cat#HB-8065 RRID:CVCL_0027
Embryonic Kidney cell line HEK-293 FT	(Meireles et al., 2017)	RRID:CVCL_6911
Embryonic Kidney cell line HEK-293 T	ATCC	Cat# CRL-1573 RRID:CVCL_0063
Experimental models: Organisms/strains		
C57Bl/6J Mice	Charles River	N/A
BALB/cJ Mice	Charles River	N/A

(*Continued on next page*)

Continued

REAGENT or RESOURCE	SOURCE	IDENTIFIER
GFP-expressing *Plasmodium berghei* ANKA-WT	(Janse et al., 2006)	Leiden Malaria Research Group line-507cl1
GFP-expressing *P. berghei* ANKA	(Janse et al., 2006)	Leiden Malaria Research Group line- 259cl2
Plasmodium berghei ANKA	(Janse et al., 2006)	Leiden Malaria Research Group- strain 2.34
P. berghei ANKA Rab5b-HA	This study	*Pb*Rab5b-HA (clone A3)
P. berghei ANKA Rab5b-mAG	This study	*Pb*Rab5b (clone A3)
P. berghei ANKA Rab5b_Q91L-mAG	This study	*Pb*Rab5b_Q91L (clone B2)
GFP and Luciferase-expressing *Plasmodium yoelii*	(Lin et al., 2011)	Leiden Malaria Research Group line- 1971cl1
Anopheles *stephensi* Mosquito	Instituto de Medicina Molecular, João Lobo Antunes	N/A
Oligonucleotides		
*Pbrab5b*_fwd- AAGCTTGCATGGGGTGTGGATCAAGTAC	This study	N/A
Primer 7-*Pbrab5b_HA*_rev- CGGCCGCGCTTATG CATAGTCCGGGACGTCATAGGGATAGCCAGCG	This study	N/A
*Pbrab5b*_3′ÚTR_forward: GGTACCTGTTTATTAC AGTGAACC	This study	N/A
Primer 2-*Pbrab5b*_3′ÚTR_reverse: AAGCTT tataaatggttacttagg	This study	N/A
Primer 6-*Pbrab5b*_5′_Integ_Forward- GCTATTTTTTTATAACGTTTTCCC	This study	N/A
*Pbrab5b*_5′_Integ_Reverse- CAAAGGAAATAAGT CATATssGCA	This study	N/A
Primer 1-*Pbrab5b*_geno_F- ATGGGGTGTGGATCAAGTAC	This study	N/A
Primer 3-*Pbrab5b*_geno_R- AAACCGTGAATAAATGTGGC	This study	N/A
Primer 8-YSN_*Pbrab5b*_mAG_5ÚTR_F- ATGGAGAGAACTAACCGATTTG	(Ebine et al., 2016)	N/A
Primer 9-YSN_mAzamiGreen_Rev- TCTAAAAT CTGCGTTCCC	(Ebine et al., 2016)	N/A
Primer 10-YSN_*Tgdhfr*_F- GGATCCCGTTTTTCTTACTT	(Ebine et al., 2016)	N/A
Primer 11-YSN_*Pbrab5b*_mAG_3ÚTR_R- GGAAT CAAAAGAAACGATACCCAC	(Ebine et al., 2016)	N/A
Primer 4-*hdhfr*_F- GTTCGCTAAACTGCATCGTC	This study	N/A
Primer 5-*yFCU*_R- GTTTGAGGTAGCAAGTAGACG	This study	N/A
*Mm*APPL1_WT_F- GCAGGTTTCTTCTGAGATGTTGGC	This study	Marino Zerial Lab
*Mm*APPL1_WT_R- GGGAACATCATGGCATCAGCAA	This study	Marino Zerial Lab
*Mm*APPL1_KO_R- TGGTTGCTGGGTATTGAACG	This study	Marino Zerial Lab
*Pb*18S forward - AAGCATTAAATAAAGCGAATA CATCCTTAC	(Slavic et al., 2016)	N/A
*Pb*18S reverse - GGAGATTGGTTTTGACGTTTATGTG	(Slavic et al., 2016)	N/A
APPL1_F_qpcr- TGCTGAACTGGATCGTAGGG	This study	N/A
APPL1_R_qpcr- CTGGAAGCAGCTATCAACCG	This study	N/A
Mmhprt forward – TTTGCTGACCTGCTGGATTAC	(Meireles et al., 2017)	N/A
Mmhprt reverse - CAAGACATTCTTTCCAGTTAAAGTTG	(Meireles et al., 2017)	N/A
Hshprt forward – TTTGCTGACCTGCTGGATTAC	(Meireles et al., 2017)	N/A
Hshprt reverse - CAAGACATTCTTTCCAGTTAAAGTTG	(Meireles et al., 2017)	N/A
Recombinant DNA		

(*Continued on next page*)

Continued

REAGENT or RESOURCE	SOURCE	IDENTIFIER
pJet 1.2	CloneJET PCR Cloning Kit. Thermo Scientific	Cat# K1231
Plasmodium expression vector (PEV)	(Setua et al., 2020)	N/A
*Pb*rab5b_HA transfection vector	This Study	N/A
*Pb*rab5b-mAG	Gift from Yumiko Saito-Nakano	(Ebine et al., 2016)
*Pb*rab5b _Q91L-mAG	Gift from Yumiko Saito-Nakano	(Ebine et al., 2016)
pUBC-mCherry-C1	Gift from Sergio Almeida	N/A
mRFP-*h*APPL1-pCNA3.1	(Erdmann et al., 2007)	Addgene #22202
mCherry-*h*Rab5a(Q79L)-pmCherry-C1	(Bohdanowicz et al., 2011)	Addgene #35138
mCherry-*h*Rab5a(S34N)-pmCherry-C1	(Bohdanowicz et al., 2011)	Addgene #35139
*Pb*Rab5b-HA- pTwist-CMV-Puro	This study	Twist Biosciences
*Pb*Rab5b(Q91L)-HA-pTwist-CMV-Puro	This study	Twist Biosciences
Software and algorithms		
Fiji	(Schindelin et al., 2012)	https://www.nature.com/articles/nmeth.2019?page=15, RRID: SCR_002285
ZEN-Blue Edition	Zeiss	https://www.zeiss.com/microscopy/int/products/microscope-software/zen.html, RRID: SCR_013672
ZEN-Black Edition	Zeiss	https://www.zeiss.com/microscopy/int/products/microscope-software/zen.html, RRID: SCR_013672
Prism	GraphPad Prism version 8.4.3for Windows, GraphPad Software, San Diego, California USA	www.graphpad.com, RRID: SCR_002798
Snapgene viewer	https://www.snapgene.com/	RRID: SCR_015052
A plasmid editor (ApE)	NA	RRID: SCR_014266
Illustrator	Adobe Illustrator 26.0.3	Adobe, RRID: SCR_010279
Other		
The Eukaryotic Pathogen, Vector and Host Informatics Resource (VEuPathDB)	https://plasmodb.org/plasmo/app/	(Amos et al., 2022)

RESOURCE AVAILABILITY

Lead contact

Further information and requests for resources should be directed to and will be fulfilled by the Lead contact, Maria M. Mota (mmota@medicina.ulisboa.pt).

Materials availability

The present study has generated novel plasmids for use in *Plasmodium berghei* as well as mammalian cells which are described in greater detail in the STAR Methods. These reagents are not deposited in public repositories but may be made available for sharing upon, personal communication.

Data and code availability

- This study has not generated novel datasets or structures.
- Custom code used in this study has been provided as Data S1.
- Any additional information required to reanalyze the data reported in this paper is available from the Lead contact upon request

EXPERIMENTAL MODEL AND SUBJECT DETAILS

Animal models

Male BALB/c wild-type mice, aged 6–8 weeks, were purchased from Charles River Laboratories (Saint-Germain-sur-l'Arbresle, France). C57BL6/J wild-type and APPL1$^{-/-}$ mice were bred in-house at the Rodent facility production area at IMM-João Lobo Antunes (IMM-JLA). APPL1$^{-/-}$ mice were generated at the laboratory of Marino Zerial (MPI-CBG, Dresden, Germany). Parental mice to establish APPL1$^{-/-}$ colonies were shipped form the animal facility of MPI-CBG and re-derived under the hygiene and procedural guidelines of the IMM-JLA Rodent facility. Mice were housed in the facilities of IMM-JLA, in specific pathogen-free environment and given water and food *ad libitum*. All *in vivo* protocols were approved by the ORBEA committee of the IMM-JLA and were performed according to national and European regulations.

Genotyping of litters from in-house breeding were performed with toe samples using the following primers: *Mm*APPL1_WT_F, *Mm*APPL1_WT_R and *Mm*APPL1_KO_R (sequences in Key resources table).

Mosquito rearing

Anopheles stephensi mosquitos were used as vectors for *P. berghei* parasites in this study. Mosquitos were bred and maintained in the insectary of the IMM-JLA. *P. berghei* infected mosquitos were maintained at 20°C in 80% atmospheric humidity, while *P. yoelii* infected mosquitos were maintained at 25°C in 80% atmospheric humidity. A 12h–12h light-dark cycle was set for the mosquito incubators. Adult mosquito diet comprised of 10% w/v glucose and 0.2% w/v para-aminobenzoic acid (PABA) in MilliQ water.

Plasmodium parasite lines

Plasmodium parasites used in this study include – *Plasmodium berghei* ANKA and *Plasmodium yoelii* 17XNL lines. *P. berghei* ANKA transgenic lines used and developed in this study are listed in the Key resources table and the generation of novel transgenic lines has been described in the STAR Methods section.

Cell lines and primary cultures

Cell lines used in this study include – HepG2 (RRID:CVCL_0027, ATCC, Manassas, VA, USA), HEK- 293T (RRID:CVCL_0063, ATCC, Manassas, VA, USA) and HEK-293FT (RRID:CVCL_6911) cells. Primary cells used in this study were murine hepatocytes from male or female C57BL/6J mice, 6–8 weeks old. The extraction and culturing techniques are described in the STAR Methods section.

METHOD DETAILS

Molecular cloning

For the generation of HA-tagged Rab5b expressing *P.berghei* parasite line, a double homologous recombination strategy was employed. The *P.berghei* rab5b (*Pb*rab5b) gene was amplified with a high fidelity polymerase (Phusion polymerase, Thermo Scientific) using the primers 1 and 2 to insert the 2x-HA tag on the *Pb*rab5b amplicon. 3′ÚTR of *Pb*rab5b gene was amplified using the primers 3 and 4. Blunt-ended PCR products were purified with QIAquick PCR purification kit (Qiagen, Hilden, Germany) and used for insertion in pJet-1.2 cloning vector (CloneJET PCR cloning kit) according to manufacturer's instructions. The ligation mixture was used for bacterial transformation of *E. coli* DH5α chemically competent cells (produced in-house according to the manufacturer's protocol, NZYCompetent Cells Preparation Buffer, NZYtech). Transformed cells were spread on LB-Ampicillin (100 μg/mL, Sigma) agar and incubated at 37°C for 16–24 h, for selection of transformants.

*Pb*rab5b-HA fragment was released from pJet1.2 backbone through digestion with *Hind*III (New England Biolabs, Massachusetts, USA) and *Not*I (New England Biolabs), as per manufacturer's instructions. The *Plasmodium* expression vector (PEV) (Setua et al., 2020) was also digested with *Hind*III and *Not*I. The digests were resolved on 1% agarose gel and the band corresponding to *Pb*rab5b-HA (1.3 kb) and the linearized PEV (4.9 kb) were excised and purified using the QIAquick Gel Extraction Kit (Qiagen). The sticky-ended DNA fragments were ligated using T4-ligase (New England Biolabs) in a molar ration of 10:1 (insert to vector) as per manufacturer's instructions. The ligation mixture was used to perform bacterial transformation as discussed previously. Transformants were screened by colony PCR (NZYTaq II master mix, Nzytech) and sub-cultured in LB-Ampicillin (100 μg/mL) broth at 37°C, 220 rpm for 16–24 h.

Plasmid DNA from transformants were extracted and purified using the NZYprep kit (Nzytech). The *Pb*rab5b-HA-PEV construct and *Pb*rab5b_3ÚTR-pJet1.2 construct were digested with *Hind*III and *Kpn*I followed by resolution on 1% agarose and purification of *Pb*Rab5b_3ÚTR band (1.02 kb) and the linearized *Pb*Rab5b-HA-PEV vector (6.2 kb). These digested fragments were ligated and transformed as described above. The final cloning vector (7.2 kb) was linearized with *Hind*III prior to the transfection of *P. berghei* merozoites.

Constructs for the generation of monomeric Azami green tagged rab5b (*Pb*rab5b-mAG) and rab5b (Q91L) mutant (*Pb*rab5b _Q91L-mAG) were a kind gift from the laboratory of Yumiko Saito-Nakano (National Institute of Health, Tokyo, Japan) (Ebine et al., 2016). Prior to transfection, the *Pb*rab5b-mAG construct was linearized with *Hind*III and *EcoR*I and the *Pb*rab5b (Q91L)-mAG construct was linearized with *Hind*III.

Primers used in the molecular cloning to generate constructs were- *Pb*Rab5b_fwd, *Pb*Rab5b_HA_rev, *Pb*Rab5b_3′ÚTR_forward and *Pb*Rab5b_3′ÚTR_reverse (sequences in Key resources table).

Plasmodium transfection

The transgenic lines used in this study were generated from the following parental strains:

1. GFP-expressing *P. berghei* ANKA (507cl1) was used for generation of Rab5b-HA expressing *P. berghei* line (*Pb*Rab5b-HA) (Janse et al., 2006).
2. *P. berghei* ANKA strain 2.34 was used for generation of Rab5b-mAG and Rab5b (Q91L)-mAG expressing *P. berghei* lines (WT and QL mutant respectively).

Transfection of *P. berghei* parasite strains were performed in blood stage merozoites as described by Janse. C.J et al. (Janse et al., 2006). Transfected schizonts were intravenously injected in Balb/c mice (6–8 weeks old). Drinking water of mice infected with transfected parasites was supplemented with pyrimethamine (70 mg/L, Sigma), at 24 h post injection for selection of transgenic parasites. The blood parasitemia in these animals was monitored through Giemsa (Sigma Aldrich) staining of blood smears (2 uL from tail vein) daily. Mice were sacrificed for blood collection upon reaching 2–5% parasitemia. Heparinized blood was either transferred to 20% glycerol-*PB*S solution for long term cold storage or used for extraction of parasite genomic DNA for genotyping of polyclonal population. Monoclonal populations of transgenic parasites were obtained through limiting dilution-based infections in Balb/c mice and following them until positive for blood stage parasites. Infected mice were sacrificed for blood collection upon reaching 2–5% parasitemia, for long-term storage and parasite genotyping to verify the insertion of transgenes in native loci.

Genotyping of transgenic parasites was performed with the following primers- *Pb*Rab5b_5′_Integ_Forward, *Pb*Rab5b_5′_Integ_Reverse, *Pb*Rab5b_geno_F, *Pb*Rab5b_geno_R, hdhfr_F, yFCU_R, YSN_*Pb*Rab5b_mAG_5ÚTR_F, YSN_mAzamiGreen_Rev, YSN_*Tgdhfr*_Rev and YSN_*Pb*Rab5b_mAG_3ÚTR_R (sequences in Key resources table).

Cell culturing and transient transfection

HepG2 cells (ATCC) and HEK-293T cells (ATCC) were cultured and maintained at 37°C, with a 5% CO_2 atmosphere, in Dulbecco's Modified Eagles Medium (DMEM, Gibco), supplemented with 10% Fetal Bovine Serum (FBS, Gibco), 2 mM glutamine (Gibco) and 100 U/mL penicillin-streptomycin (Gibco). For fluorescence microscopy analysis, cells were seeded onto No. 1 grade-12 mm diameter glass coverslips (VWR, Radnor, PA, USA) in 24-well plates (Thermo Fisher Scientific) or onto black glass-bottom 96-well plates (Greiner, Kremsmünster, Austria). Cells for immunoprecipitation or for RNA extraction workflow were seeded in 6-well plates (Thermo Fisher Scientific). Transient transfection was performed according to the manufacturer's protocol using Fugene 6 (Promega, Madison, WI, USA) and cells were cultured in antibiotic free DMEM supplemented with 10% FBS and 2 mM glutamine for 24 h at 37°C, with a 5% CO_2 atmosphere. 24 h post transfection, the culture media was replaced with DMEM, supplemented with 10% FBS, 2 mM glutamine and 100 U/mL penicillin-streptomycin.

The plasmids used for transient expression in mammalian cells were-mRFP-*h*APPL1-pCNA3.1, mCherry-*h*Rab5a(Q79L)-pmCherry-C1, mCherry-*h*Rab5a(S34N)-pmCherry-C1, *Pb*Rab5b-HA-pTwist-CMV-Puro, *Pb*Rab5b(Q91L)-HA-pTwist-CMV-Puro (details in Key resources table).

Murine primary hepatocyte extraction and culturing *in vitro*

C57BL6/J mice for extraction of liver hepatocytes were sacrificed through CO_2 narcosis followed by the rapid exposure of the abdominal cavity and cannulation of the hepatic portal vein using a 26-gauge needle. Liver perfusion medium (Gibco) at 37°C was perfused at 8–9 mL/min followed by the immediate incision of the inferior vena cava to enable drainage. The perfusion medium was allowed to flush for 10 min which was followed in concatenation with the perfusion of the liver digestion medium (37°C) at the same flow rate for 10 min with intermittent clamping of the inferior vena cava (3 s clamp every 30 s). Upon digestion, the liver was dissected into *PB*S and disintegrated with mild agitation using forceps to release the cells. The lysate was passed sequentially through 100 μm and 70 μm cell strainers and centrifuged at 50 g for 3 min. The pellet obtained was resuspended in William's medium E (Gibco) supplemented with 10% FBS and carefully pipetted into tubes containing 60% Percoll solution (1:1). Cellular fractionation was performed at 750 g at 20°C with lowest acceleration and without brakes in the centrifuge. The pellet obtained from the fractionation comprised of viable hepatocytes and was rinsed in William's medium E supplemented with 10% FBS and centrifuged at 50 g for 3 min. The resultant pellet was resuspended in William's medium E supplemented with 4% FBS, 2 mM glutamine and 100 U/mL penicillin-streptomycin. Cellular viability and yield were quantified through Trypan blue exclusion staining. Hepatocytes were seeded on either collagen coated glass coverslips (12 mm) in 24-well plates (Corning® Costar®) or 96-well plates (655090, Greiner Bio-One GmbH, Austria).

Sporozoite production

Parasites used in this study comprise of the selection marker free and GFP-expressing *P. berghei* ANKA (clone 507cl1), GFP-expressing *P. berghei* ANKA (clone 259cl2, *Pb*GFP), *P. berghei* ANKA Rab5b-HA expressing line (*Pb*Rab5b-HA), *P. b*erghei ANKA Rab5b-mAG expressing line (*Pb*Rab5b) and *P. berghei* ANKA Rab5b_Q91L-mAG expressing line (*Pb*Rab5b Q91L).

Parasites were stored in frozen blood vials at −80°C at our laboratory and contained 10^7 blood stage parasites. To achieve sporozoites, 10^7 infected red blood cells were injected intra-peritoneally into a BALB/c wild-type mouse. After 5 days of infection, exflagellation of the male gametes in the blood of infected mice was observed under a light microscope. If more than 5 events per field of view were observed, the infected mouse was used to feed naïve *Anopheles stephensi* mosquitos, for 30min. Post 22–35 days of blood meal, salivary glands containing *P. berghei* sporozoites, were dissected from infected female *Anopheles stephensi* mosquitoes into basal DMEM (Gibco) and collected into an Eppendorf tube (Eppendorf, Hamburg, Germany). Salivary glands were ground with a plastic pestle and filtered through a 40 μm Falcon cell-strainer (Thermo Fisher Scientific) to release sporozoites. Sporozoites were counted using a hemocytometer (Marienfeld Superior, Lauda-Königshofen, Germany) and were used for infection *in vivo* or *in vitro*.

Stable transfection and cell line storage

HEK-293FT cells seeded on 96-well plates 24 h prior to transfection at 70–80% confluence. Transfections were performed as per manufacturer's indications using Fugene 6 for delivery of lentiviral plasmids (Δ8.9 and VSV-G expression vectors) and respective shRNA (APPL1-non-target or APPL1 shRNA #53, #54 and #55). Cells were maintained in antibiotic free DMEM supplemented with 10% FBS and 2 mM glutamine for 24 h at 37°C, with a 5% CO_2 atmosphere.

shRNA vectors for APPL1 (Gene ID: 26060) knockdown *in vitro* were obtained from shERWOOD UltramiR Lentiviral shRNA (Transomic Technologies, Huntsville, AL, USA). Non-target, shRNA # 53 (ULTRA-3267453), shRNA # 54 (ULTRA-3267454) and shRNA # 55 (ULTRA-3267455). At 24 h post transfection, the culture media was replaced with DMEM supplemented with 20% FBS and 2 mM glutamine and 100 U/mL penicillin/streptomycin. Cell supernatant was collected 60–72 h post transfection for harvesting lentiviral particles. The supernatant was centrifuged at 1200 rpm for 5 min at RT to remove cellular debris. The supernatant was collected and aliquoted for storage at −80°C.

For stable transfection, HepG2 cells were seeded on 12-well plates at 70% confluence, 24 h prior to transfection. Transduction was initiated with replacement of cell medium with complete culture medium containing 8 μg/mL of polybrene (Sigma-Aldrich) to facilitate transduction. 100uL of freshly thawed lentviral particles were added to the primed cells and the cell-culture plate was centrifuged at 1200 g for 30 min at 37°C. 18–20 h post transduction the cell medium was replaced with fresh complete medium containing 2 μg/mL of Puromycin (Sigma-Aldrich).

The selection was performed until stabilization of cell confluency. Transgenic cells were then expanded and prepared for either cryo-storage or for experiments. Thawed transgenic cells were treated with 2 μg/mL Puromycin, prior to seeding for infection. For long-term cold storage, cells were seeded tin a T-175 flask (Thermo Fischer Scientific) at a 40% confluence in complete culture medium. Upon achieving 60–70% confluence, the cells were trypsinized (37°C, 3–4 min) and rinsed in supplemented DMEM at 1200 rpm for 5 min (RT). 5×10^6 cells were transferred to 500 uL of freezing medium (10% DMSO and 40% FBS in supplemented DMEM) in a screw capped 2 mL cryo-vial (SARSTEDT AG & Co. KG, Germany) and transferred to a pre-cooled (8°C) freezing container (Mr. Frosty, Nalgene, Sigma-Aldrich). The freezing container was transferred to −80°C cooling unit for 48 h followed by transfer of frozen vials to liquid nitrogen storage. The frozen cells were rapidly thawed at 37°C (water bath) and rinsed once in supplemented DMEM (1200 rpm, 5 min at RT) prior to sub-culturing for expansion or experiments.

Radiation inactivation of sporozoites

Freshly dissected and clarified sporozoites (in basal DMEM) in 1.5 mL microcentrifuge tubes were transferred to a sealed polyethylene bag containing 200 g of ice. The sample was then placed in the irradiator (Gammacell® 3000 Elan) and programmed for exposure to ϒ-rays at 16 kRAD for 30 min. Irradiated sporozoites were used to infect cells.

Mice infection and survival studies

For sporozoite infections, C57BL6/J mice were intravenously injected with 50,000 sporozoites, in 200 μL of basal DMEM. For the quantification of the liver burden, murine livers were collected 46 hpi in *PBS* for further processing. Estimation of parasitemia and host survival was performed by following infected mice for 7 days post infection or until they developed severe symptoms of experimental cerebral malaria (ECM), upon which they were sacrificed through cervical dislocation. Tail vein puncture was used for collection of 2 μL blood from each infected animal into 200 μL *PBS* every 24 h starting 48 hpi to follow blood parasitemia. Parasite quantification was performed by the detection of GFP positive events through flow cytometry (BD LSRFortessa, GFP 510/20 filter).

In vitro sporozoites infection

Clarified and quantified sporozoites were diluted in DMEM, supplemented with 10% FBS, 2 mM glutamine and 100 U/mL penicillin-streptomycin and added to cells seeded on either cover-slips in 24-well plates, or in 96-well plates. The plates were centrifuged at 3000 rpm for 5 min at RT to facilitate settling of floating sporozoites. Cells were incubated at 37°C, with a 5% CO_2 and humidified atmosphere for 2 h following which the medium was replaced to fresh supplemented DMEM containing 50 μg/mL Gentamycin (Gibco) and 0.85 μg/mL Amphotericin B (Gibco). Cells were incubated at 37°C, with a 5% CO_2 and humidified atmosphere. Infected cells were fixed at relevant time-points for microscopic examination.

Drug treatments in infected cells

Infected HepG2 cells were treated with small molecules to study the effect of APPL1 distribution around the EEF. Cytoskeletal disruption was performed using Cytochalasin D (Sigma) for host actin and Nocodazole (Sigma) for host microtubules. Treatment was performed in cell culture medium for 75 min at 37°C and 5% CO_2 in a humidified atmosphere (Grützke et al., 2014). *Plasmodium* PI4K inhibition driven blockade of PVM protein export was performed with 200 nM KDU-691 (Sigma) in the cell culture medium. Treatment duration was either 6–24 hpi followed by replacement of drug free medium, or from 24-48 hpi (Hanson et al., 2013; McNamara et al., 2013).

Sample preparation for estimation of parasite burden

Murine livers were collected at 46 hpi in *PB*S, followed by the separation of the left liver lobe from the rest. The left liver lobe was drop fixed in 4% paraformaldehyde in *PB*S (NZYtech, Lisboa, Portugal) for 2 h at room temperature followed by incubation at 4°C overnight. Fixed tissues were preserved in 0.1% Sodium Azide- *PB*S buffer (pH7.4) at 4°C for sectioning and detection of EEFs via immunofluorescence.

The remaining lobes were transferred to 3 mL of denaturing solution (4 M guanidium thiocyanite (Sigma), 25 mM sodium citrate (Sigma), 0.5% *N*- lauroylsarcosine (Sigma) and 0.7% β-mercaptoethanol in MilliQ water treated with DEPC (Sigma) containing 0.1 mm Zirconia/Silica beads (Biospec™ Products, Bartlesville, OK, USA). Liver homogenization was performed through mechanical disruption in a Mini-BeadBeater (BioSpec Products) for 1 min. 200 μL of tissue lysate was transferred to a clean 1.5 mL microcentrifuge tube (Eppendorf) for extraction of total RNA, using NZY Total RNA Isolation Kit (NZYTech, Lisboa, Portugal), as per manufacturer's instructions. Cultured cells were lysed *in situ*, 46–48 hpi with the lysis buffer of the NZY Total RNA Isolation Kit, supplemented with 1% v/v β-mercaptoethanol. RNA extraction was performed using the same kit, according to manufacturer's protocol. Quantification of total RNA concentration was performed on NanoDrop 2000 spectrophotometer (Thermo Fisher Scientific) according to the manufacturer's guidelines.

cDNA synthesis was performed with 1 μg of purified RNA using the NZY First-Strand cDNA Synthesis Kit (NZYTech), as per manufacturer's instructions. cDNA was then used for quantitative Polymerase Chain Reaction (qPCR) using iTaq Universal SYBR Green Supermix (Bio-Rad Laboratories, Hercules, CA, USA). Measurements of SYBR fluorescence were performed on ViiA 7 (384-well plates) Real-Time PCR Systems (Thermo Fisher Scientific). Relative abundance of *Pb*18s RNA with respect to *MmHprt* RNA was quantified through the $\Delta\Delta C_T$ method:

$$\Delta C_t = C_t^{Gene\ of\ interest} - C_t^{Housekeeping}$$

$$\Delta\Delta C_t = \Delta C_t^{Experimental} - \Delta C_t^{Control}$$

$$Relative\ Gene\ expression = 2^{[\Delta\Delta C_t]}$$

Mice transcardial perfusion

For immunofluorescence microscopy of host endosomes in infected murine tissue, the livers were collected upon transcardial perfusion 46–48 hpi. Mice for transcardial perfusion were sacrificed via CO_2 narcosis until the subsiding of thoracic and abdominal breathing. The animal was then prepared for transcardial perfusion as described by Gage.G et al. (Gage et al., 2012). The perfusion was performed directly with the fixative solution (4% paraformaldehyde (*PF*A) and 0.1% Tween 20 in *PB*S (pH 7.4)) at a flow rate of 4 mL/min directly for 10 min at RT. Livers were then excised wholly and transferred to fresh fixative solution and incubated at 4°C overnight with rotation. Fixed livers were then transferred to a storage solution comprising 0.1% Sodium Azide in *PB*S (pH7.4).

Murine liver cryosection

Transcardially fixed tissues were rinsed in *PB*S for 15 min for 5 times at RT. Rinsed samples were cut into smaller pieces and dehydrated by incubation in 30% w/v sucrose solution in *PB*S, at 4°C until the tissue pieces had sunk. Peel away tissue molds (VWR) were pre-cooled on ice followed by addition of O.C.T medium (Tissue-Tek, Sakura Finetek, USA). Dehydrated tissue pieces were dried on tissue and pre-dipped in O.C.T, followed by gentle insertion into the tissue mold ensuring that the flat edge rested perpendicularly to the base of the mold. O.C.T medium was gently added to fill the mold and the sample was cooled in dry ice until complete solidification of the O.C.T medium. These tissue blocks could be stored for long term at −80°C. Sectioning of tissue blocks were performed on a Cryostat (Microm HM 560, Thermo Fisher Scientific) equilibrated with the knife at −15°C and block holder at −18°C. Sections of 10 μm were semi-automatically cut and collected on Super Frost Plus Slides (Thermo Scientific). The slides were stored at −20°C or prepared for immunofluorescence staining.

Murine liver floating section

Fixed tissues were rinsed in *PB*S buffer for 15 min, 5 times at RT. The tissue was cut into smaller pieces and excess buffer was drained on filter paper. The tissue pieces were embedded in 4% w/v Agarose -*PB*S solution (maintained at 60°C in a water bath) on peel away tissue molds. The tissue was maintained on ice until solidification of the embedding medium. The tissue-agarose blocks were

released from molds and mounted on the stage of a vibrating blade sectioning machine (Vibratome VT 1000S, Leica Biosystems, Germany). The tissue was sliced semi-automatically in 50 μm slices and each section was transferred to a well in a 48 well plate, containing 0.1% w/v Sodium Azide-*PB*S. Agarose films from each section was carefully removed under a stereoscope. These sections were either stored at 4°C or processed immediately for immunofluorescence staining.

Sample preparation for immunofluorescence assay and live fluorescence imaging

Immunofluorescence assay was performed in murine liver sections, primary hepatocytes and HepG2 cells. Glass slides with cryosections were thawed on ice, followed by equilibration at RT. After desiccation the tissue fragment was demarcated by a paraffin marker. The sections were then gently washed twice in *PB*S at RT. Aldehyde residues were quenched by incubation in 0.1% w/v Glycine (Sigma)-*PB*S solution followed by permeabilization in 0.3% v/v Triton X-100 (USB corporation, Cleveland, USA)- *PB*S buffer (*PB*STx) for 10 min at RT. Permeabilized sections were rinsed thrice in *PB*S, followed by blocking in 3% w/v Bovine Serum Albumin (BSA) (NZYTech, Lisboa, Portugal)-*PB*S solution. Incubation with primary antibodies was performed by diluting respective antibody in the blocking solution and incubating at 4°C overnight. Incubated samples were rinsed thrice in 0.1% *PB*STx at RT. Secondary antibody (and/or dyes) were diluted in the blocking solution and sections were incubated for 90 min at RT, followed by three washes in 0.1% *PB*STx, then in *PB*S. Sections were mounted in 50 μL mowiol solution (Sigma-Aldrich) and covered with No.1.5 precision cover glass (0.17 ± 0.005 mm) (Marienfeld, Lauda-Königshofen, Germany) and allowed to dry in the dark for 12–16 h.

Sections in 48-well plates were rinsed twice in *PB*S. Residual aldehydes were quenched by incubation in 0.1% Glycine-*PB*S solution followed by permeabilization in 0.5% *PB*STx for 1 h at RT. Primary antibodies were diluted in TxB buffer (0.2% gelatin (Sigma), 300 mM Sodium Chloride (Sigma) and 0.3% Triton X-100 in *PB*S) and 250 uL was added per well. Plates were sealed with paraffin films and incubated for 12–16 h at RT with gentle rocking. Tissue sections were then rinsed 0.3% *PB*STx (5×, 5 min) at RT with rocking. Secondary antibodies were diluted in TxB buffer and 300 uL was added per well. Plates were sealed with paraffin films and incubated for 12 h at RT with rocking. Stained sections were rinsed 0.3% *PB*STx (5×, 5 min) at RT with rocking, followed by three washes in *PB*S. Tissue slices were transferred to a glass slide and excess liquid was drained with filter paper. Each slice was fenced with double sided tape followed by mounting in Fluoromount G (Thermo Fisher Scientific) mounting medium. Mounted slides were covered with No.1.5 precision cover glass (0.17 ± 0.005 mm) and allowed to dry in the dark for 12–24 h.

Cells for immunofluorescence assay (primary hepatocytes and HepG2 cells) were prepared by removing the cell culture media, followed by gentle rinsing in *PB*S twice at RT. Fixation of cells was performed in either 4% PFA-*PB*S solution for 15 min, RT or in ice-cold methanol-acetone cocktail (1:1) for 5 min at −20°C. Fixed cells were washed thrice in *PB*S at RT. Permeabilization was performed in 0.1% *PB*STx for 5 min at RT. For partial permeabilization protocols, 0.01% Saponin-PBS was used for 15 min at 4ºC. Permeabilized cells were washed thrice in *PB*S at RT, followed by blocking in 3% BSA-*PB*S for 20 min at RT. Primary antibodies were diluted in blocking solution and 25 uL was either spotted on a paraffin film or was added directly to a well of a 96-well plate. Coverslips with seeded cells were lifted from 24-well plates, mildly drained and mounted upon the antibody cocktail spotted on paraffin film. Samples were incubated at 4°C, overnight. Samples were then rinsed thrice in *PB*S at RT followed by incubation in secondary antibody (and/or dyes) for 90 min at RT. Stained cells were rinsed thrice in *PB*S followed by mounting in Fluoromount G on glass slides for coverslips or directly in wells of a 96-well plate. Mounted samples were allowed to dry in the dark for 12–16 h.

Primary antibodies used for fluorescence microscopy include: goat α *Pb*UIS4 (AB0042-200, Sicgen, Cantanhede, Portugal), rabbit α APPL1 (ABS314, Merck Millipore, Massachusetts, USA), rabbit α APPL1 (Miaczynska et al., 2004), rabbit α Rab5 (Bucci et al., 1994), rabbit α monomeric Azami-green (PM052M, MBL International Corporation, Massachusetts, USA), rat α HA (clone 3F10, 11867423001, Roche) and rat αTubulin (Edgar Gomes Lab, IMM JLA, Lisbon, Portugal).

Secondary antibodies and dyes used for fluorescence microscopy include Alexa-488 dye conjugated donkey α goat IgG (A32814, Invitrogen), Alexa-647 dye conjugated donkey α rabbit IgG (A32795, Invitrogen), Alexa-594 dye conjugated donkey α rat IgG (SA5-10028, Invitrogen), Alexa-555 dye conjugated donkey α mouse IgG (A32773, Invitrogen), Hoechst 33342 (H1399, Invitrogen) and Alexa-555 conjugated Phalloidin (A34055, Invitrogen).

For live imaging experiments, HepG2 cells were seeded on a 35 mm μ-Dish (ibidi, Wisconsin, USA) with treated polymer coverslip. 24 h after transient transfection of mRFP-APPL1, cells were infected with *Pb*Rbab5-mAG or *Pb*Rbab5 (Q91L)-mAG sporozoites as described previously. Infected cells were imaged 44 hpi in phenol red-free complete DMEM (high glucose, HEPES) supplemented with 2 mM glutamine, 100 U/mL penicillin-streptomycin and 10% FBS.

Microscopy

Samples for quantification of parasite numbers or quantification of signals at the PVM were imaged using the inverted Zeiss Cell Observer Microscope (ZEISS, Jena, Germany) with 40× EC Plan-NeoFluar Air objective (ZEISS) and images were acquired on the ZEISS Axiocam 506 mono CCD camera. Image acquisition was performed in a semi-automatic fashion. Position specified imaging and auto-focus of the microscope was controlled by the ZEN Blue software (ZEISS). Fixed samples for signal co-localization studies and/or structural localization/resolution were imaged on point-scanning confocal microscopes (ZEISS-LSM 880 or ZEISS-multiphoton Microscope). The magnification used was 63×, Plan-Apochromat DIC 1.4 oil immersion or LCI Plan-Neofluar 1.3 Gly/water immersion (ZEISS). Imaging setup was performed on ZEN 2.3 SP1 (ZEISS) software with a pixel dwell time 4–6 μsec averaged 2–4 times with a voxel size of 0.1 μm * 0.1 μm * 0.3 μm. Live imaging was performed on point-scanning confocal microscope (ZEISS-LSM 880) with 63× magnification objective (Plan-Apochromat DIC 1.4 oil immersion) in a temperature (37°C) and CO_2 (5%) controlled hu-

midified micro-chamber. *Pb*Rbab5-mAG EEFs (WT or Q91L) in mRFP-APPL1 expressing cells were imaged using the Fast Airyscan modality of the LSM 880 microscope (Huff, 2016). The time-lapse was acquired with an interval of 10 min over a span of 180–240 min and averaged twice. The acquisition settings were performed on ZEN 2.3 SP1 (ZEISS) with a voxel size of 0.07 μm * 0.07 μm * 0.2 μm.

Structured illumination microscopy (SIM)

HepG2 cells were infected with *Pb*Rab5b_HA parasites in 96-well imaging plates as described previously. Infected cells were fixed at 48 hpi in ice-cold methanol-acetone cocktail and prepared for immunofluorescence staining as previously described. SIM imaging of *Pb*Rab5b_HA infected cells was done using Nikon Ti eclipse system equipped with Andor N-SIM. Images were acquired in four channels with z-slices corresponding to a thickness of 2 μm with a 100× SR Apo TIRF 1.49 NA objective using NIS Elements AR 4.4 and Andor iXon EMCCD3, 897 cameras. 3D reconstruction was performed using NIS elements AR software with default parameters.

Sample processing for correlative light and electron microscopy (CLEM)

C57BL6/J mice were infected with 50,000 *Pb*GFP sporozoites intravenously and at 46 hpi prepared for transcardial perfusion as described previously. The CLEM fixative (4% PFA and 0.01% glutaraldehyde in 200 mM HEPES in MillQ H_2O, pH 7.4) was perfused at 4 mL/min using a peristaltic pump for 10 min at RT. The fixed liver was then dissected and incubated in the CLEM fixative overnight at 4°C with gentle rotation. Overnight fixed livers were rinsed thrice in *PB*S and stored in 1%-PFA solution in 100 mM HEPES (PFA/HEPES), at 4°C. Liver lobes were cut to smaller pieces and sectioned on Leica VT 1200 s vibratome (Leica Biosystems, Nussloch, Germany) in ice cold 100 mM HEPES buffer to obtain 80-100 μm sections. Parasite localization was performed from the residual GFP signal in these sections on a fluorescence dissection microscope, where regions containing 1–2 parasites were excised manually. Samples were then stored in PFA/HEPES solution at 4°C prior to high pressure freezing.

Single liver sections were transferred to the recess (100 μm) of lecithin coated 3 mm copper/gold carriers and closed with plane lids. The carrier was over-filled with 20% polyvinylpyrrolidone in 100 mM HEPES buffer and air bubbles were removed by gentle tapping prior to closing the lid. The samples were frozen at > 2100 bar pressure with a cooling rate of >20,000 K/s using the Leica EM HPM100 machine (Leica Microsystems, Wetzlar, Germany) and either stored in cryo-tubes in liquid nitrogen or directly transferred into the Leica EM AFS2 machine (Leica Microsystems) for freeze substitution.

Freeze substitution and embedding of the samples in LR white (London Resin Company Ltd. England) was performed according to previously published protocols (Markert et al., 2016, 2017). Briefly, they were transferred to the AFS2 freeze in the freeze substitution cocktail (0.1% KMnO4 in anhydrous acetone) at – 90°C for 65 h with a change of the solution after 24 h. The temperature was raised to 45°C, over 11.25 h (4°C/h) and maintained at - 45°C for 6 h during which eight washes were performed: four times with pure acetone over the course of 4 hours, then with acetone/ethanol (3:1 and 1:3 v/v) for 30 min each. Two final washes were performed with pure ethanol and the temperature was raised up to +4°C (4°C/h; 16 h). A 1:1 mixture of LR White/ethanol was left overnight (16 h, 4°C), followed by 3 washes with 100% LR White (1 h, 4 h, 16 h) and embedding in gelatine capsules (Size 0). Polymerisation was at 42°C for 3 days or until cured.

Serial sectioning was done using a Leica EM UC7 ultramicrotome (Leica Microsystems) and a histo Jumbo diamond knife (DiATOME). The 100 nm thick sections were collected on poly-L-lysine coated glass slides (Thermo Fisher) that were submerged into the trough of the diamond knife.

Sections were briefly stained with Hoechst (1:10,000 in *PB*S, 10 min) and screened for the identification of the specimens and only the sections of interest were immunolabelled. Rehydration was done in blocking solution (0.1% BSA, 0.05% Tween 20 in 0.05 M Tris buffer, pH 7.6) for 10 min. The primary antibodies were diluted 1:500 (polyclonal goat anti-UIS4, Sicgen, catalog number AB0042-200; rabbit α APPL1, developed at the lab Marino Zerial, MPI-CBG, Dresden, Germany) in blocking solution and applied to the sections for 30 min in a dark humid chamber. Sections were then washed with tris buffer (0.05 M Tris-HCl, 0.15 M NaCl, pH 7.6) five times for 5 min each. The secondary antibodies were incubated sequentially starting with donkey anti-goat (Jackson Immunoresearch, 705-545-003), followed by rinsing and incubation goat anti-rabbit (Jackson Immunoresearch, 111-585-144) and methyl green (1:10,000 of 2% in H_2O) (Prieto et al., 2015) in the blocking solution and applied to the sections for 30 min in the dark. Samples were washed with tris buffer followed by a final rinse in distilled water. Excess fluids were drained on tissue and the samples were mounted on high precision cover glasses (Marienfeld, Lauda-Königshofen, Germany) with Mowiol for SIM imaging.

Workflow for correlative light and electron microscopy (CLEM)

Light imaging of the parasites for CLEM was performed with a Zeiss Elyra S.1 SIM (Structured Illumination Microscope), with serial sections being tracked manually. Once the imaging of the fluorescent signals was complete, the coverslips were detached form the slides and Mowiol was washed off with water. The slides were dried and cut into smaller pieces to fit into the SEM. Sections were then contrasted for 15 min with 2.5% uranyl acetate in ethanol (filtered), washed with 100% ethanol, 50-50% ethanol-water and water followed by incubation for 10 min in 50% Reynolds' lead citrate (in water) and final washes with water and dried with compressed air. The glass pieces were attached to SEM specimen holders and silver paint was applied to minimize charging and to electrically couple the surface of the glass with the specimen holder. They were then coated with a 5 nm carbon layer to prevent charging during SEM imaging. The scanning electron microscope (SEM) images were obtained on a SEM (JSM-7500F, JEOL) using a LABe (Low-Angle Backscattered electrons) detector. Acquisition was performed with the image rotation software feature to compensate

for deviations in section orientation, enabling consistency during subsequent alignment, correlation and 3D-reconstruction steps. Image processing and correlation have been described later in this section.

Immunoprecipitation

Immunoprecipitation (IP) studies were performed in two experimental regimes. The first comprised of HepG2 cells, infected with *Pb*Rab5b-HA parasite line (1:1 multiplicity of infection) and processed 48 hpi. The second experimental setup comprised of HEK-293T cells either untransfected or transfected with constructs expressing–HA only (pCMV-HA)/*Pb*UIS4 (cytosolic domain)/*Pb*Ra5b_HA/*Pb*Rab5b_Q91L_HA according to the manufacturer's protocol using Fugene 6 (Promega, Madison, WI, USA). Transfected cells were processed 48 h post transfection. Cells were lysed in IP lysis buffer (50 mM Tris-HCl-pH 7.5, 5 mM EDTA, 150 mM NaCl and 1% Triton X-100), containing freshly added protease inhibitors (cOmplete, EDTA-free Protease Inhibitor cocktail, Roche, Basel, Switzerland). The lysate was centrifuged at 13,000 g for 10 min at 4°C, and the supernatant was used for pre-clearance with unconjugated protein A/G-plus agarose beads (sc-2003, Santa Cruz, Heidelberg, Germany). A sample of 30 μL of this lysate was stored at −80°C, to be used as input. Protein A/G-plus agarose beads were cross-linked with the respective primary antibody (rabbit αAPPL1 (ABS314, Merck Millipore) using 1% v/v glutaraldehyde (Sigma-Aldrich) in cross-linking buffer (20 mM Na_2HPO_4, 5 mM NaH_2PO_4. 0.2 M NaCl and 0.5 mM EDTA in MilliO H_2O) at 4°C and then used to pull down APPL1 or *Pb*Rab5b-HA from the pre-cleared lysate (Sinz, 2010). Elution was performed with 50 μL of 1% w/v sodium dodecyl sulphate (SDS) in *PB*S. The IP elute, beads, post-IP supernatant and input were treated with Laemmli buffer (NZYtech) and incubated at 95°C for 5 min. The denatured samples were resolved on a 10% denaturing polyacrylamide gel (SDS-PAGE) and processed for western blotting as described below.

SDS-PAGE and western blotting

Cells for western blotting of phosphorylated proteins were lysed *in situ* with 50mM Tris-HCl (pH 8.0), 150 mM NaCl, 5mM EDTA, 1% (v/v) NP-40, 1 mM Na_3VO_4, 10 mM NaF, 10 mM NaPyroph, 1 mM 4-(2-aminoethyl) benzenesulfonyl (AEBSF), 10 μg/mL leupeptin, 10 μg/mL aprotinin, 1 μg/mL Pepstatin, on ice for 20 min. Lysates were collected in 1.5 mL microcentrifuge tubes and centrifuged at 13,000 g at 4°C for 10 min. The supernatants were transferred to fresh 1.5 mL microcentrifuge tubes and protein quantification was performed according to the manufacturer's guidelines using the BCA method (Pierce BCA protein assay kit). 30 μg protein was denatured in Laemlii buffer (NZYtech) at 95°C for 10 min and subsequently resolved in 10% polyacrylamide gel.

Cells for western blotting of IP experiments were lysed, processed and proteins were denatured as previously described. Denatured lysates were resolve on 10% SDS-polyacrylamide gel in Tris-Glycine-SDS buffer (25 mM Tris, 192 mM glycine, 0.1% SDS, pH 8.3) (Bio-Rad, California, USA) at 60 V for 30 min followed by 90 V for 90 min at RT. Proteins were transferred to 0.2 μm nitrocellulose membranes (Bio-Rad) using wet-transfer in Towbin buffer (25 mM Tris, 192 mM Glycine and 20% methanol in ddH_2O). Membranes were blocked in 5% BSA-1%Tween-*PB*S buffer (*PB*ST) at RT for 60 min, with rocking. Membranes were then incubated with the appropriate primary antibodies, diluted in 1% *PB*ST, for overnight at 4°C. Membranes were washed with 1% *PB*ST, 3 times for 10 minutes (RT) followed by incubation in the appropriate secondary antibodies (conjugated to Horseradish peroxidase) diluted in 1% *PB*ST, for 45–60 min at RT. Membranes were washed again 3 times for 10 minutes (RT). Western blots were developed using Immobilon ECL Ultra Western HRP Substrate (Merck Millipore) on either ChemiDoc XRS + system (Bio-Rad) or using X-ray films (AGFA, Mortsel, Belgium) in Curix developers (AGFA).

The primary antibodies used for probing membranes were- goat α *Pb*UIS4 (AB0042-200, Sicgen), rabbit α APPL1 (ABS 314, Merck Millipore), rabbit α HA (clone C29F4, Cell Signaling Technology, Danvers, MA, USA), rabbit α mCherry (ab167453, abcam, Cambridge, UK), rabbit α phospho-Akt (S473) (9271, Cell Signaling Technology), rabbit α phospho-GSK-3β (S9) (5558, Cell Signaling Technology), rabbit α phospho-AMPK (T172) (2535, Cell Signaling Technology), rabbit α total Akt (9272, Cell Signaling Technology), rabbit α total GSK-3β (12456, Cell Signaling Technology), rabbit α total AMPK (2603, Cell Signaling Technology and mouse α actin (ab8224, abcam). The secondary antibodies used were: goat α mouse IgG F(ab')2, polyclonal antibody HRP conjugate (BML-SA204-0100, Enzo Life Sciences, Lausen, Switzerland), goat α rabbit IgG, HRP-linked Antibody (7074, Cell Signaling Technology), mouse α rabbit IgG HRP-linked Antibody (Rabbit TrueBlot, Rockland Immunochemicals, Inc. Pennsylvania, USA), rat α mouse IgG HRP-linked Antibody (Mouse TrueBlot, Rockland Immunochemicals, Inc), and rabbit α goat IgG HRP-linked Antibody (81–1620, Thermo Fisher Scientific).

QUANTIFICATION AND STATISTICAL ANALYSIS

Statistical analysis

Statistical analyses were performed using GraphPad Prism software-version 8.4.3 (GraphPad, LA, Jolla, CA). Student's t Test and Mann-Whitney *U*-test were used to assess significance of differences at 99% confidence intervals, between two groups depending on sample size. p-values for each set of analyses have been specified in respective figure legends.

Image analysis

All immunofluorescence images were acquired using Zen 2 (blue edition, ZEISS) or Zen 2.3 SP1 (black edition, ZEISS) softwares. Post-processing for Fast-Airyscan images was performed on Zen 2.3 SP1. Other images were processed using FIJI software (version 1.53g) (Schindelin et al., 2012). Semi-automatic quantification on FIJI was performed with a custom macros script, which was modified for each image set accordingly. For visualization and processing of DNA gels, the software ImageLab (Bio-Rad, California, USA) was used (version 5.2.1). Image panels or artwork for graphical visualization were prepared on Adobe Illustrator CS6- version 16 (Adobe Systems Incorporated, California, USA).

Intensity quantifications have been reported either as Integral fluorescence intensity (IFI) which refers to the total intensity values in a region of interest (*Pb*UIS4 marked region) or as Mean fluorescence intensity (MFI) where the total intensity of a region of interest (IFI) is normalized to the area of this region. The macro code used for this quantification is reported in supplemental information.

The correlation of the fluorescence (SIM) and SEM images was done manually with the free vector graphics editor inkscape (version 0.91, https://inkscape.org) flowing our previously described protocol of unbiased correlation using independent intrinsic landmarks (Markert et al., 2017). In short, all images were loaded into the window and the fluorescence images were stacked together, hiding all channels beneath the Hoechst/methyl green track to allow unbiased correlation. The stack was grouped, the aspect ratio locked, and the transparency was set to 50–60%, depending on the image quality. DNA stain was used as a landmark in both the SIM and SEM images, for subsequent correlation. Upon achieving the best possible fit, the channels were unlocked, the images cropped, and exported for merging. The merge was done with the free software GIMP (GNU Image Manipulation Program, version 2.10, https://www.gimp.org).